Vol. 17 • No. 33 • August 19 • 2021

www.small-journal.com

NANO · MICRO

small

WILEY-VCH

NANO · MICRO small
www.small-journal.com

Ultralow Resistance Two-Stage Electrostatically Assisted Air Filtration by Polydopamine Coated PET Coarse Filter

Enze Tian, Qipeng Yu, Yilun Gao, Hua Wang, Chao Wang, Yinping Zhang, Baohua Li, Meifang Zhu, Jinhan Mo, Guiyin Xu,* and Ju Li**

Airborne particulate matters (PM) pose serious health threats to the population, and efficient filtration is needed for indoor and vehicular environments. However, there is an intrinsic conflict between filtration efficiency, air resistance, and service life. In this study, a two-stage electrostatically assisted air (EAA) filtration device is designed and the efficiency-air resistance-filter life envelope is significantly improved by a thin coating of polydopamine (PDA) on the polyethylene terephthalate (PET) coarse filter by in situ dopamine polymerization. The 8 mm thick EAA PDA-140@PET filter has a high filtration efficiency of 99.48% for 0.3 µm particles, low air resistance of 9.5 Pa at a filtration velocity of 0.4 m s^{-1}, and steady performance up to 30 d. Compared with the bare PET filter, the penetration rate for 0.3 µm particles is lowered by 20×. The coated PDA is of submicron thickness, 10^{-3} × the gap distance between filter fibers, so low air resistance could be maintained. The filter shows steadily high filtration efficiency and an acceptable increase of air resistance and holds nearly as many particles as its own weight in a 30 day long-term test. The working mechanism of the EAA coarse filter is investigated, and the materials design criteria are proposed.

1. Introduction

Airborne particulate matters (PM) pose serious health threats to the population because they can reach the thoracic region and bloodstream, increasing the risk of dementia, respiratory and cardiovascular diseases, and mortality.[1–4] With increasing air pollution caused by industry, transportation, and wildfires (e.g., in Australia, California, and Siberia recently), PM removal has become an ever more important human adaptation strategy to a changing environment. Since most people spend more than 80% of their time indoors,[5] efficient indoor PM removal devices have become essential, and a high airflow rate is required in many scenarios.

Fibrous filtration is widely used for indoor ventilation systems. However, there is an intrinsic conflict between filters' high filtration efficiency, low air resistance, and long service life (i.e., large dust-holding capacity while maintaining filtration efficiency and air resistance). High-efficiency air filtration usually has large air resistance, which costs up to 50% in acquiring the electricity to drive fans. Moreover, it has short service life since the air resistance builds up steeply from the beginning as the filter gets clogged by the PM dust loading.[6] For decades, considerable efforts have been made to develop novel filter materials such as nanofibers and electret fibers.[7–11] Nanofibers decrease the air resistance by introducing a slip-effect when the fiber diameter is smaller than the mean free path of air molecules (≈65 nm).[10–12] Electret fibers enhance the filtration efficiency by introducing an electrostatic effect through charging the fibers with corona plasma charging, triboelectrification,

Dr. E. Tian, Dr. Q. Yu, Dr. H. Wang, Dr. C. Wang, Dr. G. Xu, Prof. J. Li
Department of Nuclear Science and Engineering
and Department of Materials Science and Engineering
Massachusetts Institute of Technology
Cambridge, MA 02139, USA
E-mail: xuguiyin@mit.edu; liju@mit.edu
Dr. E. Tian, Y. Gao, Prof. Y. Zhang, Dr. J. Mo
Department of Building Science
Tsinghua University
Beijing 100084, China
E-mail: mojinhan@tsinghua.edu.cn
Dr. E. Tian, Y. Gao, Prof. Y. Zhang, Dr. J. Mo
Beijing Key Laboratory of Indoor Air Quality Evaluation and Control
Beijing 100084, China
Dr. Q. Yu, Prof. B. Li
Shenzhen Key Laboratory on Power Battery Safety Research
and Shenzhen Geim Graphene Center
Tsinghua Shenzhen International Graduate School
Shenzhen 518055, China
Dr. Q. Yu
School of Materials Science and Engineering
Tsinghua University
Beijing 100084, China
Prof. M. Zhu
State Key Laboratory for Modification of Chemical Fibers
and Polymer Materials
College of Materials Science and Engineering
Donghua University
Shanghai 201620, China

The ORCID identification number(s) for the author(s) of this article can be found under https://doi.org/10.1002/smll.202102051.

DOI: 10.1002/smll.202102051

or electrospinning.[13–15] However, though frequently used in personal respirators, filters made of nanofibers still usually have relatively high air resistance and short service life when being applied in building ventilation systems.[16] And the benefit of electret filters is limited when the electret charges are degraded by environmental aging.[17,18] Therefore, developing high-efficiency airborne PM filtration technology with minimal air resistance and long service life (weeks to months) remains a great challenge.

To overcome the challenge, continuous electrostatic charging of the airborne PM and/or the filter material was proposed as a promising method.[19–29] Most of these trials are however based on medium-high efficiency filters. These filters are either thin membranes to have limited dust-holding capacity or have equivalently >50 Pa air resistance at 1 m s^{-1} filtration velocity. Tian and Mo developed an electrostatically assisted air (EAA) filtration technology by the synergistic effect of a corona charging field (electrodynamic) and a polarizing field (electrostatic).[20] An approach to improving the performance of EAA filtration is loading high dielectric constant inorganic particles on polyurethane (PU) foams by adhesive.[30] However, this adhesive method requires base filters of large pores to avoid the adhesive blocking the airways. Since large pores would let certain particles bypass the collecting media, the highest filtration efficiency for 0.3–0.5 μm particles was less than 90%.[30] Furthermore, coating inorganic particles causes a significant decrease in filter flexibility.[31]

This work aims to improve the EAA filtration performance by modifying the coarse PET filter, which achieved the highest filtration efficiency in the previous study. The thick, coarse PET filters are expected to have a lower pressure drop and larger dust-holding capacity than that of thin dense filters. A key challenge is how to add electrostatic responsive material to PET bulk filter thoroughly, uniformly, and firmly. To achieve that, we proposed to coat polydopamine (PDA) on the PET coarse filter (PDA@PET) by an in situ dopamine polymerization process. We demonstrated a novel EAA PDA@PET filter, which had attractive attributes of high filtration efficiency, low air resistance, and long service life. We found that the in situ coated PDA increased the roughness of PET fiber surfaces, therefore promoted the particle-fiber adhesion and enhanced the filtration efficiency. The PDA clusters grew to the submicron scale, which was just one-thousandth of the gap distance between filter fibers, so the low air resistance of the base filter could be maintained. In addition, PDA is found to exhibit superior electrostatic properties and dust-holding capacity to achieve high and steady electrostatic filtration efficiency. By controlling the surface microstructure of filters with an optimized amount of added precursor, we reported an EAA PDA-140@PET filter with a high filtration efficiency of 99.48% for 0.3 μm particles, as well as a low air resistance of 9.5 Pa at 0.4 m s^{-1} filtration velocity. Compared with the untreated bare PET filter, for 0.3 μm particles, the penetration rate was lowered by 20 × and the quality factor (QF) was enhanced by 119%, respectively. The filter showed steady high filtration efficiency (averaging 98.63%, 99.04%, and 99.83% for 0.3, 0.5 and 1 μm particles) and an acceptable increase of air resistance (9.5 to 17.4 Pa) in a 30 d long-term test.

2. Results

2.1. Design of EAA Coarse PET Filters Coated with PDA or PVDF

Figure 1a shows the schematic of the designed EAA filtration device and the details are included in the "Experimental Section". In brief, there are two externally applied voltages used in the two-stage EAA device: U_1 in stage I is for generating a corona discharge that allows a particle that flies through it to gain net charge eq_p, where e is the elementary charge and q_p has a distribution that depends on the particle characteristics including particle diameter d_p, and U_1. Then, this (q_p, d_p) particle flies into stage II, where together with the filter fibers, will be subjected to an $E_2 = U_2/D_2$ polarizing electric field. D_2, the distance between the two mesh electrodes in stage II, will be sufficiently long to prevent any dielectric breakdown discharge (unlike stage I). E_2 promotes 10^2 μm ranged interactions between the polymer fiber and the (q_p, d_p) particle, as well as between the particles (recall Faraday's electric field-line experiment on forming chains of dielectric particles),[30] so it becomes easier for the particles to find a fiber surface and attach to it, as well as to agglomerate with other particles and form "dust clusters."[30] Given that we would like to operate the filter in high air velocity mode, the dust clusters will be subjected to large shear forces, and may become resuspended if the few Å-ranged particle–polymer adhesion is not strong enough. Thus, surface engineering of filter fibers to enhance the long-duration adhesion (up to weeks, and even when U_1 and U_2 are turned off) between the dust cluster and fiber surface is crucial, to prevent dust cluster resuspension and enhance dust-storage capacity. Furthermore, the coated fiber must be such that the 10^2 μm ranged dielectric attraction is not diminished, as this is the first step toward building dust agglomerate on the fiber surface.

Thus, we propose that the rational design principles for EAA filters with ultralow resistance at relatively high filtration velocity should be:

(a) large open pores on the order of ≈10^2 μm to reduce air resistance. This would enable air resistance below 10 Pa at an air filtration velocity of tens of cm s^{-1}, with a ≈1 cm thick, 200 g m^{-2} filter.
(b) significant E_2 that penetrates the ≈1 cm thick filter interior to cause "Faraday agglomeration" across such ≈10^2 μm pore distance, which we have previously demonstrated with multiple dust particles being observed to form chains, using in situ optical microscopy.[30] This also requires a strong dielectric response of the fiber in the range of diameter, e.g., ≈10^1 μm.
(c) a small and perhaps nonlinear electronic conductivity (I–V relation) of the fiber to have reasonable antistatic property,[33,34] so while the monopolar charge q_p of a dust particle enhances its long-range interaction with the fiber, such monopolar charge gets released over a timescale of minutes to hours, allowing this dust particle to later dielectrically bind with other dust particles, which originally carried the same-signed charges.
(d) fiber diameter on the order of ≈10^1 μm, with the expectation that it may become 2 × or 3 × thicker with dust coverings after long-term filtration operation. Ideally, we would like

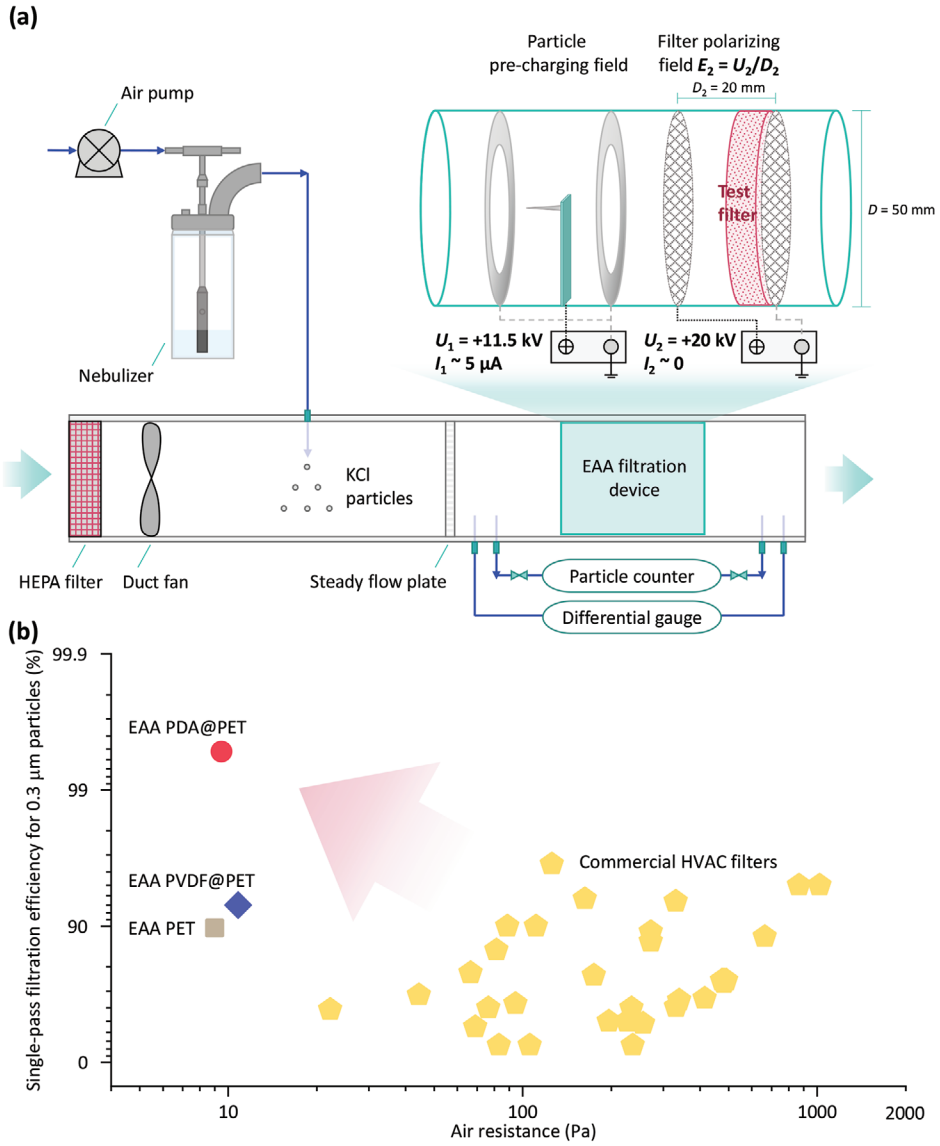

Figure 1. Filtration test apparatus and performance comparison. a) Schematic of experimental apparatus for the particulate matter filtration test of the two-stage EAA filter. b) Performance comparison of EAA PET filter, PVDF-120@PET filter, PDA-140@PET filter, and non-EAA commercial HVAC filters.[32] If the experiments were not conducted at 0.4 m s^{-1} face air velocity, we calculated the equivalent air resistance by assuming that air resistance was proportional to face air velocity.[6] Source data are provided in Table S1 (Supporting Information).

the filter to be able to trap as much dust as its own weight, meaning ≈10^2 g m^{-2} dust-holding capacity. Given the density of the in situ formed dust layer must be quite low compared to the polymer density (tap density of a powder), this implies more than 4 × nominal fiber volume expansion, an incredible dust-holding ability that we will demonstrate later in this paper.

(e) few Å-ranged strong adhesion between a dust cluster/layer with the fiber surface, so once adhered, it will hold and the dust cluster/layer does not easily come off in shear flow. Both the chemistry and morphology of the surface matter in this aspect, as is well-known in adhesion mechanics. In addition, such adhesion strength could be sensitive to the particle characteristics and humidity in the air.

Accordingly, to discover the most effective material for EAA filters, we started with the nonconductive PET coarse filter, which had achieved the highest single-pass filtration efficiency and low air resistance in the previous study.[20] We chose ≈10^2 μm coarse filter because conventional high-efficiency filters (like nanofibrous filters) with a high packing density have a very high air resistance, low dust-holding capacity, and early clogging.[17,35–37] We believe that coarse filters with large pores would promote in-depth filtration, maintaining a lower air resistance with the continued PM accumulation.

The methods for coating substrates with hetero-material have been developed for years, such as adhesion,[30] electrospinning,[38] blow-spinning,[39] dip-coating,[40] calcination,[41] and physical vapor deposition.[42] Among them, we chose dip-coating

to modify the PET coarse filters, as it has great advantages in coating uniformly on large coating areas and allowing for easy and quick large-scale industrial manufacture.[43] Noticing that it is difficult for inorganic matter and organic polymers to combine firmly, we coated polymer on the PET coarse filter. One selected polymer is polyvinylidene fluoride (PVDF), a dipolar material demonstrated as an effective material to fabricate electret filters.[8,10,11,44] Nanofiber filters made of PVDF have achieved the highest filtration efficiency among polyacrylonitrile (PAN), polyvinylpyrrolidone (PVP), polystyrene (PS), polyvinyl alcohol (PVA), polypropylene (PP), polyamide-6 (PA6), and polyurethane (PU).[7,10] The other selected polymer is polydopamine (PDA), which is an environmentally friendly and versatile adhesive for surface modification. By simply dipping objects in an aqueous solution of dopamine, thin and surface-adherent PDA coating can be formed onto a wide variety of organic and inorganic materials by autopolymerization.[45] Moreover, it was realized in a facile and environmentally friendly process, which can be conducted in a basic environment without using or producing harmful products.[46] Though the basic polymerization mechanism is not fully discussed here, PDA-based materials have rapidly advanced in recent years for applications in energy, biomedical science, sensing, and water treatment.[47] However, such promising materials have not been applied in air filtration. The molecular models of the different polymers are shown in Figure S1 (Supporting Information).

Figure 2a presents an overview of the preparation of PDA-coated PET (PDA@PET) filters. We indexed PDA@PET filters by different amounts of precursor addition. For example, PDA-140@PET denotes 140 mg dopamine (as a precursor) being added to the 60 mL solution during the in-situ polymerization process. Similarly, we obtained PVDF coated PET (PVDF@PET) filters. Details of the preparation process are in the "Experimental Section".

2.2. Characterization of the Filters

Figure 2b,c and Figures S2–S4 (Supporting Information) show optical photographs and scanning electron microscopy (SEM) images of the bare PET filter, PVDF@PET, and PDA@PET filters, and pure PDA. Compared with the bare PET filter, the PDA clusters are generated and uniformly distributed on the surface of PET fibers. The larger the dopamine addition is, the more PDA clusters form on the fiber surfaces, roughening the fiber surface and making the filters darker in color. The size of PDA cluster (<1 μm) is more than 10 times smaller than the fiber diameter (20–30 μm), and the fiber diameter is approximately 10 times smaller than the gap between fibers (≈200 μm). Figures S5 and S6 (Supporting Information) show the energy dispersive spectroscopy (EDS) elemental mappings of PVDF-120@PET and PDA-120@PET filters. Interestingly, being different from PDA in situ polymerization process, PVDF films form and distribute irregularly between the gaps among PET fibers.

As shown in the Fourier transform infrared (FTIR) spectra (Figure S7, Supporting Information), the characteristic band of 1504 cm^{-1} from the spectrum of pristine PDA, ascribed to C=N stretching vibration,[48] was found on the spectra of PDA@PET filters. Meanwhile, pristine PVDF shows peaks at 1180 and 1401 cm^{-1}, which are consistent with symmetric and asymmetric C−F_2 stretching modes for β phase PVDF.[49] But the two peaks were not found on the spectra of PVDF@PET filters. The spectra of PDA and PVDF@PET filters are very close to the spectra of bare PET filter, indicating that the coatings do not change the main functional groups of the bulk filter material. The X-ray diffraction (XRD) patterns in Figure S8 (Supporting Information) reveals that the diffraction peaks of the bare PET filter are sharp and intense, indicating its crystalline nature. The coatings of PDA and PVDF do not change much of the bare PET's diffraction peaks, but make it more amorphous. Thermogravimetric analysis (TGA) and differential scanning calorimetry (DSC) results in Figures S9 and S10 (Supporting Information) illustrate that all PDA@PET and PVDF@PET filters are thermodynamically stable in the general building environment (<40 °C).

In EAA coarse filters, the U_1, U_2-dependent electrostatic filtration efficiency is much higher than the mechanical filtration efficiency ($U_1 = U_2 = 0$).[20,23] Therefore, the electrical properties of filters, including the dipole moment, relative dielectric constant, and initial surface potential, are important in enhancing the electrostatic filtration efficiency.[50] The dipole moments, which indicate the polymer's polarity, were calculated as 2.93, 1.85, and 3.25 D for the repeating units of PET, PVDF, and PDA, respectively. The relative dielectric constants (ε_r), which indicate how easily each polymer can become polarized by an imposed electric field, were tested as 1.26, 6.86, and 5.74 at 1 MHz for the PET fiber, pure PVDF, and PDA. And ε_r of the coated filters was tested as 1.32 and 1.52 for PVDF-120@PET and PDA-120@PET filters. By using an atomic force microscope (AFM), it was observed in Figures S11 and S12 (Supporting Information) that the PDA coated surface was rougher and exhibited greater absolute surface potential value compared to the bare PET surface.

2.3. Influence of Coatings on Performance

As the minimum filtration efficiency is generally known to occur in the vicinity of 0.3 μm for most fibrous filters,[51] we first compared the filtration efficiency and penetration rate for 0.3 μm particles of the filters. The single-pass filtration efficiency of particles with a certain size of d_p (μm) was calculated by:

$$\eta(d_p) = \left(\frac{C_{up}(d_p) - C_{down}(d_p)}{C_{up}(d_p)} \right) \times 100\% \quad (1)$$

where C_{up} and C_{down} are the particle count (pcs) at the upstream and downstream of the filter, respectively. The penetration rate $p(d_p)$ is defined as 1-$\eta(d_p)$. We use the symbol $\eta_{0.3}$ and $p_{0.3}$ to denote $\eta(d_p = 0.3\ \mu m)$ and $p(d_p = 0.3\ \mu m)$.

As shown in **Figure 3**a, PET, PVDF-40@PET and PDA-40@PET filters showed $p_{0.3}$ of 99.28%, 97.99% and 94.64% when $U_1 = U_2 = 0$, that is, almost all particles escaped the filter. With U_1 and U_2 turned on, the filters' $p_{0.3}$ showed a sharp decline to 10.34%, 9.24%, and 1.77%, respectively. This result demonstrates that electrostatic capture dominates in the overall filtration process of an EAA coarse filter. Moreover, coating PDA on

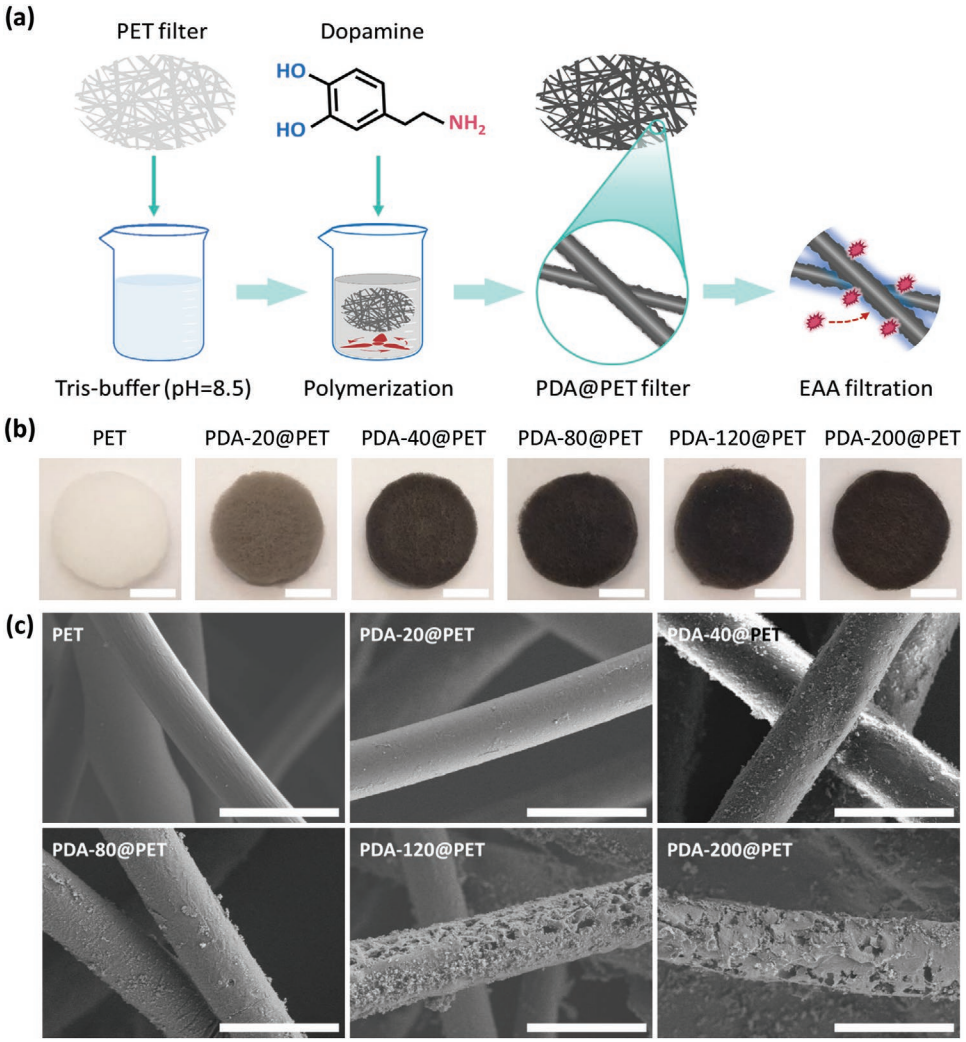

Figure 2. Preparation method and morphology of bare PET and PDA@PET filters. a) Schematics showing the preparation of PDA@PET filters by in situ polymerization coating. b) Digital images and c) SEM images of bare PET and PDA@PET filters with different precursor adding amount. Scale bars, 20 mm in (b) and 50 µm in (c).

the PET filter showed superior performance than coating the PVDF with the same weight of precursors (40 mg). The EAA PDA-40@PET filter showed less than one-fifth $p_{0.3}$ of that of the PVDF-40@PET filter. Similarly, as shown in Figure 3b, PVDF-120@PET and PDA-120@PET showed $p_{0.3}$ of 95.51% and 94.22% with $U_1 = U_2 = 0$, indicating that the mechanical filtration efficiencies of the two filters are close. With U_1, U_2 turned on, their $p_{0.3}$ dropped to 7.02% and 0.76%, respectively, confirming the superior performance of EAA PDA-120@PET filter. Figure 3c shows $\eta_{0.3}$ of PDA@PET filters with different precursor adding amounts. With the largest precursor adding amount, the PDA-200@PET filter achieved the highest $\eta_{0.3}$ at 99.61% with U_1, U_2 turned on.

Figure S13 (Supporting Information) shows the air resistance of PVDF@PET and PDA@PET filters with different precursor loading. The bare PET filter had a low air resistance of 9.0 Pa at 0.4 m s^{-1} air filtration velocity. After dip-coating, the air resistance of PVDF-120@PET and PDA-120@PET filters increased to 10.8 and 9.8 Pa, respectively. PVDF@PET filters showed higher air resistance because PVDF films formed between the gaps among the PET fibers (as shown in Figures S4 and S5, Supporting Information) and blocked the airflow pathway a bit more. By contrast, the air resistance of PDA@PET filters was not affected by the submicron-thick layer of PDA, as shown in Figure 2c and Figure S6 (Supporting Information).

Generally, a high filtration efficiency η (or a low penetration rate p) is traded off by high air resistance, and therefore high energy consumption of the driving fan. To account for both filtration efficiency and air resistance, we used the quality factor (QF) to evaluate the overall filter performance, defined as:

$$\mathrm{QF}(d_p) \equiv \frac{-\ln\left(1-\eta(d_p)\right)}{\Delta P} \tag{2}$$

where $\mathrm{QF}(d_p)$ refers to QF (Pa^{-1}) for particles with a specific diameter of d_p (µm). We use the symbol $\mathrm{QF}_{0.3}$ to denote $\mathrm{QF}(d_p = 0.3\ \mu m)$.

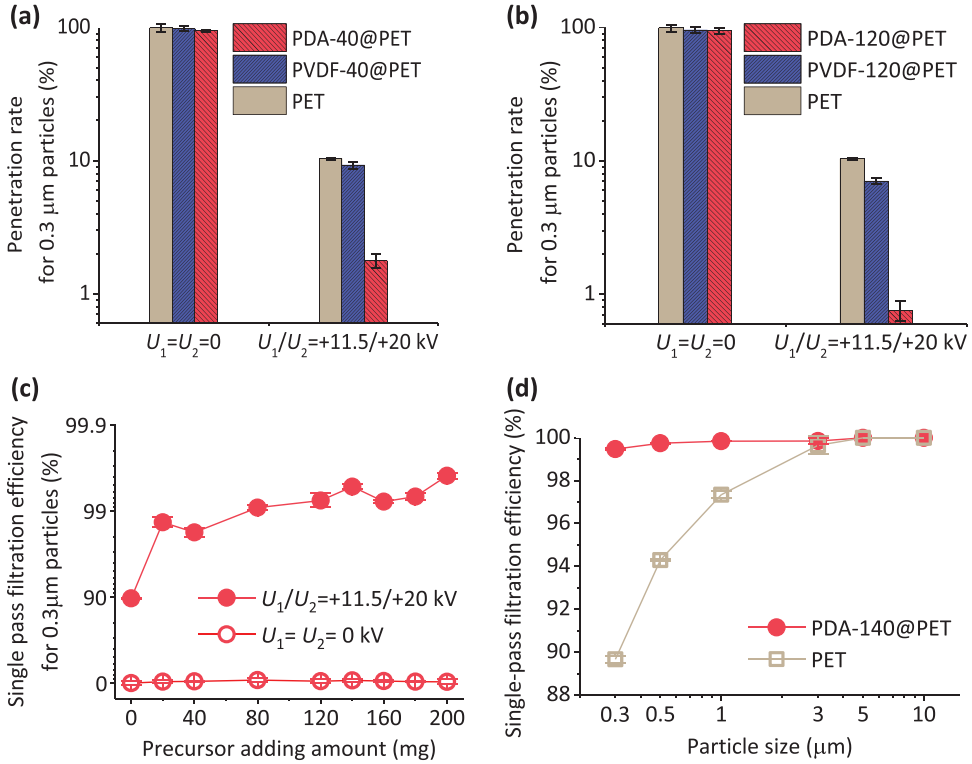

Figure 3. Filtration performance of bare PET, PVDF@PET, and PDA@PET filters. a,b) Penetration rates for 0.3 μm particles of bare PET, PVDF@PET, and PDA@PET filters with the EAA filter device's U_1, U_2 on or off. c) Single-pass filtration efficiencies for 0.3 μm particles of PDA@PET filters with different precursor adding amount and U_1, U_2 on or off. d) Comparison of PET and PDA-140@PET filters in single-pass filtration efficiencies for 0.3–10 μm particles (U_1, U_2 on). All error bars in (a–d) are the standard deviations of six observations of the experiments.

As shown in Figure S14 (Supporting Information), EAA filters with U_1, U_2 on showed superior $QF_{0.3}$ than the original filters (U_1 = U_2 = 0). For example, $QF_{0.3}$ of the bare PET filter increased 313 times from 0.0008 to 0.252 Pa^{-1} by lifting U_1 and U_2 from 0 to +11.5 and +20 kV, respectively. Although coating PVDF resulted in a slightly increased $\eta_{0.3}$, it also caused a larger air resistance. Consequently, the $QF_{0.3}$ of EAA PVDF-120@PET filter is 0.246 Pa^{-1}, which was even lower than the EAA bare PET filter. By contrast, EAA PDA@PET filters showed the highest $QF_{0.3}$ at 0.553 Pa^{-1} for EAA PDA-140@PET filter. This was because when the precursor (dopamine) adding amount increased from 40 to 200 mg, $\eta_{0.3}$ of EAA PDA@PET filter increased from 98.23% to 99.61%, while the air resistance increased from 9.3 to 11.5 Pa. Thus, EAA PDA@PET filter achieved relatively high filtration efficiency with relatively low air resistance and reached the best performance with an optimal precursor adding amount (140 mg). In the following sections, we chose EAA PDA-140@PET filter to study its performance further.

2.4. Initial Performance of the EAA PDA-140@PET Filter

Both d_p = 0.3 μm and larger particles should be considered for their single-pass filtration efficiency. For example, SARS-CoV-2 was mainly found in droplet particles with two size ranges: 0.25–1 μm and >2.5 μm.[52] Thus, we further discussed the single-pass filtration efficiency distribution for d_p = 0.3–10 μm particles. As shown in Figure 3d, the EAA filtration efficiencies of both bare PET and PDA-140@PET filters increased as particle size enlarged. But the filtration efficiency gap between the two filters became smaller as particle size enlarged. For example, for 0.3 μm particles, the EAA filtration efficiencies of bare and PDA-140@PET filter were 89.66% and 99.48%, respectively, while for 3 μm particles, 99.65% and 99.85%, respectively.

High efficiency at a high air filtration velocity is expected to meet the demand in building and vehicular ventilations. When evaluating the air resistance of a filter, the filtration velocity across the filter should be considered, as it is directly correlated with the air resistance.[6] As shown in **Figure 4**a, with an increasing filtration velocity, the EAA filtration efficiencies of both bare PET and PDA-140@PET filters dropped. At 3.8 m s^{-1} filtration velocity, the bare PET filter only showed 56.71% in $\eta_{0.3}$. By contrast, the PDA-140@PET filter maintained 76.91% in $\eta_{0.3}$ at 3.7 m s^{-1} filtration velocity. The air resistances of both bare PET and PDA-140@PET filters, as shown in Figure 4b, increased as filtration velocity grew. And the difference between the two filters in air resistance was small. For example, the air resistances of the bare PET filter and the PDA-140@PET filter were 220 and 215 Pa at 3.7–3.8 m s^{-1} filtration velocity, respectively. In conclusion, PDA-140@PET filter showed the superiority of an enhanced filtration efficiency with basically the same air resistance compared with the bare PET filter.

Since the base PET filter in this study is a coarse filter, PDA@PET filters have low air resistance, which is important

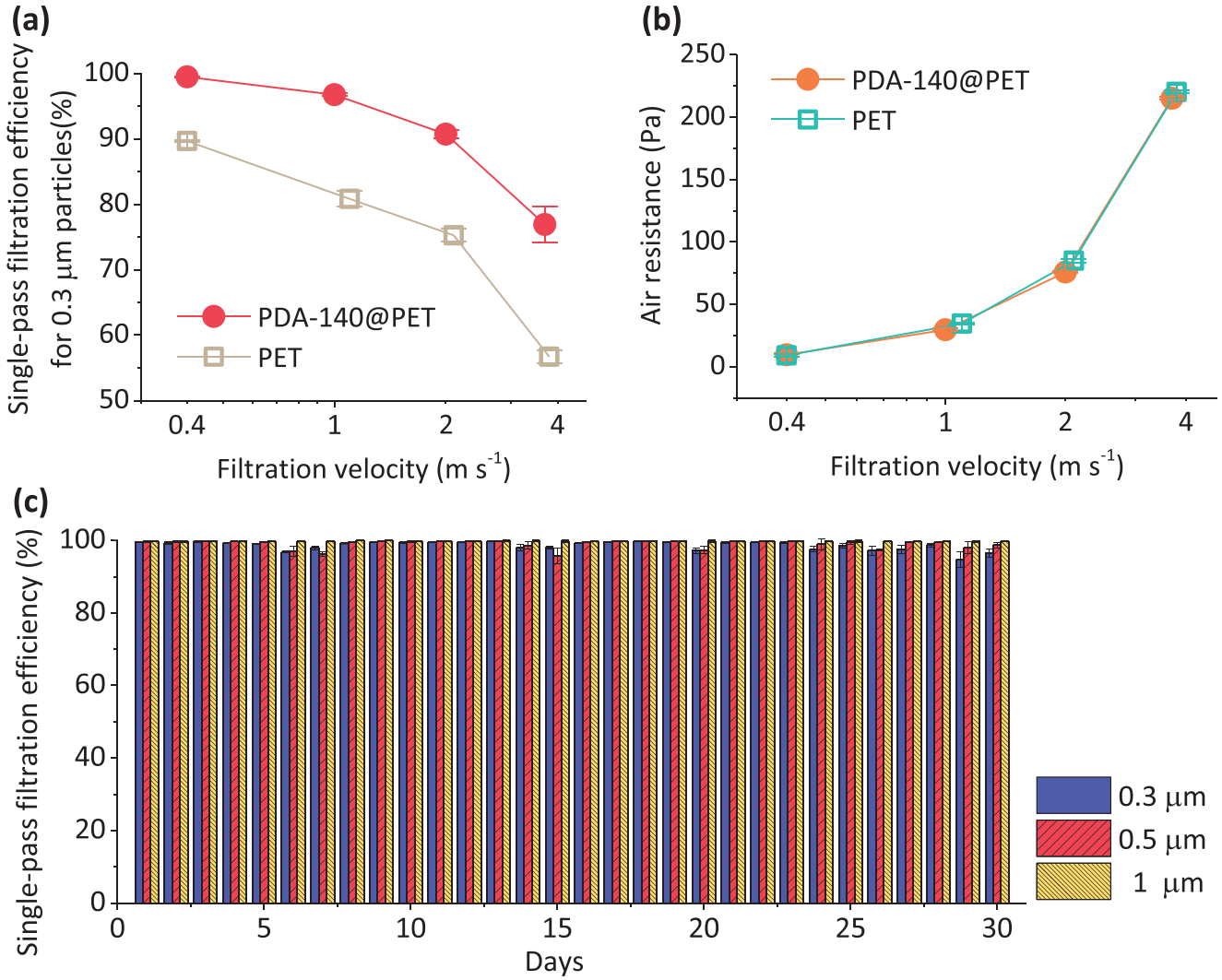

Figure 4. Filtration performance of EAA bare PET and PDA-140@PET filters. Comparison of EAA PET and PDA-140@PET filters in a) single-pass filtration efficiencies for 0.3 μm particles and b) air resistance at air filtration velocities from 0.4 to 4 m s^{-1}. All error bars in (a,b) are the standard deviations of six observations of the experiments. c) Long-term single-pass filtration efficiencies of EAA PDA-140@PET filter for 0.3–1 μm particles. The error bars are the standard deviations of 27 observations of the experiments in each day.

for energy saving. We compared the performance of EAA filters and commercial HVAC filters in Figure 1b. The detailed information for the commercial filters is listed in Table S1 (Supporting Information). EAA PET and PVDF@PET filters have remarkably lower pressure drop than commercial HVAC filters when achieving similar filtration efficiency as theirs. The commercial HVAC filters which had the highest filtration efficiency for 0.3 μm particles of 96.5% cost 125.7 Pa air resistance—which is >13 × that of the EAA PDA-140@PET filter's. Furthermore, EAA PDA-140 filter showed much higher filtration efficiency ($\eta_{0.3}$ = 99.48%) with such remarkably lower air resistance (9.5 Pa at 0.4 m s^{-1} filtration velocity).

2.5. Long-Term Performance of the EAA PDA@PET Filter

As the filtration performance should sustain the continuous loading of pollutants in real applications, improving the long-term performance of filters (weeks and months) is important for relieving environmental burdens and saving maintenance cost of building ventilation systems. In this study, we measured the long-term performance of the EAA PDA-140@PET filter for 30 d. We continuously ran the filtration apparatus for 8 h each day, and obtained the daily filtration efficiencies by an average of nine tests. The environmental and operating parameters, including air temperature, relative humidity, particle concentration, particle accumulating amount, and corona charging current, are available in Figure S15 and Table S2 (Supporting Information). As shown in Figure 4c, the single-pass filtration efficiencies for 0.3, 0.5, and 1 μm particles remained at very high levels of averaging 98.63%, 99.04%, and 99.83%, respectively. The variation of filtration efficiency is caused by the fluctuation of air temperature, moisture, particle concentration, and accumulation.[19] It is shown in Figure S16 (Supporting Information) that the PDA-140@PET filter is insensitive to moisture when the air moisture content is below

9.5 g kg^{-1} (equally 48% relative humidity at 25 °C, or 65% relative humidity at 20 °C). SEM images in Figure S17 (Supporting Information) show the morphology of the PDA-140@PET filter after the long-term testing. Particles tended to form dust clusters or layers on the fiber surface. Generally, particle accumulating on the filter fibers and blocking the airways limit the service life of the filter material by the build-up of air resistance.[53] However, in the 30 d running, though the air resistance of the PDA-140@PET filter increased from 9.5 to 17.4 Pa, it is still far lower than equally high-efficiency commercial filters (>100 Pa at equal air filtration velocity).[32] Compared with a commercial pleated electret filter which served the same period (Table S3, Supporting Information),[19] the EAA PDA-140@PET filter showed higher average filtration efficiency and lower air resistance. In all, the EAA PDA-140@PET filter showed steady high filtration efficiency and an acceptable air resistance increase in a 30 day long-term running period, thus gave a superior performance to ventilation filtrations.

We compared the long-term performance of the EAA PDA-20@PET and PDA-200 PET filter using high concentration (Figure S18, Supporting Information) feeding particles, to see whether the filters would fail. As shown in Figures S19 and S20 (Supporting Information), although the two filters exhibited nearly the same $\eta_{0.3}$ at the beginning (PDA-20@PET filter: 94.80%, PDA-200@PET filter: 94.84%), the PDA-200@PET filter ended up with higher $\eta_{0.3}$ (94.79%) than the PDA-20 PET filter (89.69%). This indicated that PDA@PET fibers with larger coating amounts would have more rough surfaces and therefore exhibited the superior dust-holding capacity to adhere charged particles firmly. **Figure 5**a shows that after 30 d running, massive dust layers accumulated on the filters (132.6 g m^{-2} for PDA-20@PET and 173.9 g m^{-2} for PDA-200@PET filter), making the fibers become more than 2 × thicker in diameter with particle coverings. As the starting weight of the PDA-20@PET and PDA-200@PET filters were 171.6 and 187.9 g m^{-2}, the dust-holding amount was amazingly on the same order as the filter's own weight (dust loading 77 wt% and 93 wt%, respectively), without sacrificing the high filtration efficiency and ultralow resistance characteristics, over a period of 30 d. We compared $\eta_{0.3}$ of the PDA-20@PET and PDA-200@PET filters in more conditions (i.e., U_1/U_2 being turned on or off, and charging pins/filter being "clean" or "dirty," or no filter installed) in **Table 1**.

3. Discussion

In conventional filters, improving filtration efficiency is the result of enhancing mechanical filtration by blocking airways, which increases the air resistance as a trade-off and gives an adverse effect on energy saving, as well as on the dust-holding capacity. Electret filters have also been widely used to enhance the overall filtration efficiency without increasing air resistance by introducing an electrostatic effect to the particle capture process. For electret filters with high filtration efficiency and long-serving life, materials with high surface potential and superior dust-holding capacity are preferred. The two characters are related to the fiber electrical properties, including dielectric constant,[54,55] conductivity,[56,57] and the spatial distribution of dipoles and free charges.[57–60] The influence of materials properties is still under debate. For example, Liu et al. reported that polymers with higher dipole moment would have higher particle filtration efficiency since they can have stronger dipole–dipole and induced-dipole intermolecular forces toward the polar functional groups presented at the outer surface of the particles.[7] Cai et al. compared the filtration efficiency of electrospun filters with similar structure and found that a higher relative dielectric would lead to higher filtration efficiency, while the polymer with a higher dipole moment not necessarily has higher filtration efficiency in all cases.[61] But the electret–dust interaction is relatively weak as it is an electric dipole-induced dipole interaction when the dust particle does not have monopolar charge, so the particle capture distance R_C is not very large (perhaps few μm), restricting the effective pore size. Empirically, existing electret filters have high resistance due to small pore size approximately few μm, and poor dust-holding capacity.

Our EAA coarse filter has fiber diameters $\approx 10^1$ μm and large pore size $\approx 10^2$ μm, which gives the ultralow resistance, but very poor mechanical filtration efficiency when $U_1 = U_2 = 0$. However, the filtration efficiency rises to an excellent level when U_1 and U_2 are turned on (Table 1). We see huge improvements even with $U_2 = 0$ and just U_1 on, with efficiency up to ≈90% (depending on whether the stage-I corona charge pins / stage-II filter is "clean" or "dirty," i.e., already covered with dust or not; and often "dirty" is better than "clean"). This means if $q_p(U_1) > 0$, even with $E_2 = 0$, there is sufficient electrical interaction to cause a charged particle to get close to a fiber within few-Å distance and adhere. We call this the monopole capture (MC) effect, that is, a charge monopole $q_p(U_1) > 0$ strong enough to increase a dust particle's capture cross-section with a fiber greatly. We believe this is because if $q_p(U_1) = 0$, a charge-neutral suspended particle will largely follow the air streamlines in laminar flow (the Reynolds number $Re = 0.4\ m\ s^{-1} \times 100\ \mu m / 1.5 \times 10^{-5}\ m^2\ s^{-1} = 2.7$), and since the air streamlines avoid the fiber surface, it is unlikely for a charge-neutral particle to come close enough (within few-Å distance) to get adhered. But once $q_p(U_1) > 0$, there is monopole-induced dipole electrostatic interaction with additional force $F_E = q_p(U_1)E_{local}$ that causes the particle trajectory to break away from the air streamlines, and be attracted to some surfaces. Even with $U_2 = 0$, the range of E_{local} can be on the order of $\approx 10^1$ μm, i.e., the fiber diameter, since the interaction force between a monopole and its induced dipole moment on a fiber would scale inversely to the third power of the distance normalized by the fiber diameter. We call this the "monopole capture distance," $R_{MC}(U_2 = 0; q_p)$, if without U_2. Once the $E_2 = U_2/D_2$ polarizing electric field is turned on, $R_{MC}(U_2; q_p)$ can increase further as the range of E_{local} is further increased. Indeed, far away (more than $\approx 10^1$ μm distance) from any fiber, the monopole would still be accelerated by $q_p(U_1)E_2$ and accumulate momentum, which is crucial for it to break away from the air streamlines later to impact a fiber surface, like a car running too fast could break from a curvy road and hit trees. Thus, with U_2 going from 0 to 20 kV, we expect $R_{MC}(U_2; q_p)$ to potentially go from $\approx 10^1$ to $\approx 10^2$ μm. The efficacy of such $\approx 10^1$ to $\approx 10^2$ μm ranged electrostatic capture has been demonstrated by in situ optical microscopy.[30] R_{MC} would also depend on the coating material and dielectric/pyroelectric/electret heterogeneity, as

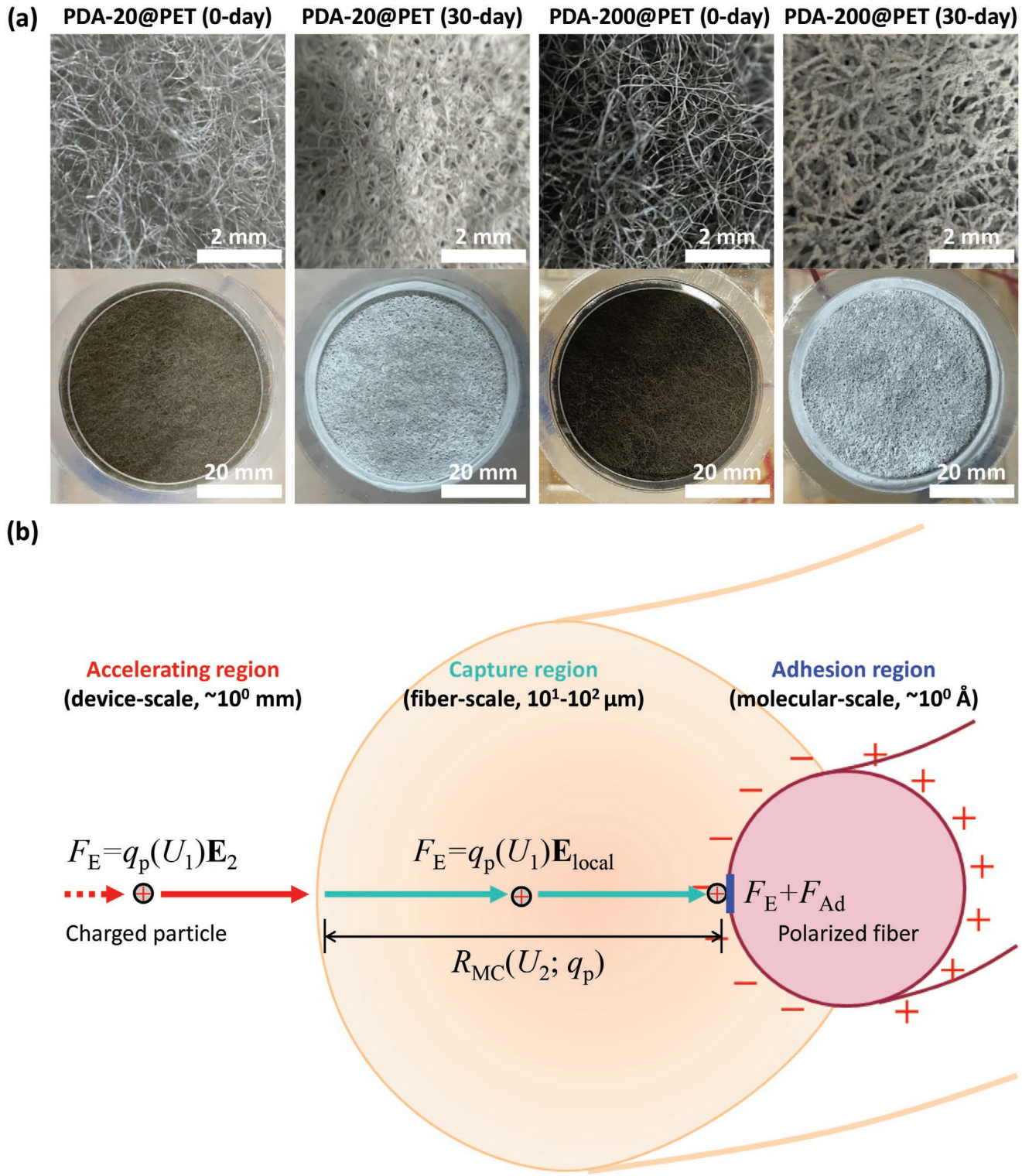

Figure 5. a) Digital images of PDA-20@PET and PDA-200@PET filters before and after 30 d running. b) Schematic of enhancing filtration efficiency of air coarse filter by electrostatic and adhesion effect in three regions.

these factors could modify E_{local} when ≈10^1 µm away (see in Figure 5b).

Not every particle that hits a fiber surface would stick, however. In surface science, there is the important concept of "sticking probability," originally defined for molecules. The dust particle needs to dissipate its kinetic energy and come to a full stop on the fiber surface, despite the air shear flow—otherwise, the particle could bounce back to the stream. And

Table 1. Single-pass filtration efficiencies of EAA PDA@PET filters for 0.3 µm particles when stage-I corona charging pins/stage-II filter is "clean" or "dirty," or no filter installed in stage II. We use the symbol PDA20 and PDA200 to denote PDA-20@PET and PDA-200@PET filter, respectively. Clean and dirty charging pins were shown in Figure S21 (Supporting Information), while clean and dirty filters were shown in Figure 5a.

U_1/U_2 [kV]	0/0		0/+20		+12/0		+12/+20	
Charging pin, filter status	PDA20	PDA200	PDA20	PDA200	PDA20	PDA200	PDA20	PDA200
Clean, none	0.28%	0.13%	8.48%	7.77%	73.16%	76.15%	74.91%	77.83%
Clean, clean	15.82%	9.65%	23.80%	16.99%	77.00%	85.30%	94.80%	94.84%
Clean, dirty	33.28%	35.13%	46.31%	43.81%	90.59%	92.85%	93.53%	94.08%
Dirty, none	0.14%	0.33%	3.63%	5.03%	48.97%	40.92%	51.47%	43.97%
Dirty, clean	1.43%	0.75%	14.72%	13.76%	53.96%	53.91%	61.29%	66.35%
Dirty, dirty	40.13%	43.62%	49.33%	48.07%	85.54%	91.54%	89.69%	94.79%

since the surface sites may be covered by other particles that may carry the same-signed residual charge, there is a chance of monopole-monopole repulsion that destabilizes the adhesion. It is conceivable that a particle could hit multiple fibers before coming to a stop; it is also conceivable that a particle or particle cluster already stationary on a fiber could get fragmented and resuspended. Most will get recaptured again while a small fraction escapes the filter. Generally speaking, polymer fibers can have the antistatic property that causes monopole charge leaking. Without draining away the monopole charges from connected fibers to the ground electrode, there will inevitably be Coulomb explosion (electrostatic energy divergence) in the filter with the accumulation of charged dust particles—one can compute the capacitance of the entire stage-II filter with respect to stage-I, and conclude that monopole charge leaking from stage-II filter material back to stage I (can be through the ground currents) must occur on the timescale of minutes in order to prevent large electrostatic potential build-up between them, in our two-stage electrostatic filtration device. Monopole charge leaking would enhance the sticking probability, and stabilize dust clusters and agglomerates seen in Figure 5a. Indeed, after 30 d, there are so much dust agglomerations that the filter has changed color, and the fibers have thickened to 4× the original volume as seen in optical and SEM images due to the loose packing of the accumulated dust. While increasing the air resistance moderately, the dust-coated "dirty" filter seems to attract and retain fresh dusts as well as, or sometimes even better than, the "clean" filter (Table 1), which is surprising and impossible to achieve without the antistatic monopole charge leakage mechanism.

Strong adhesion F_{Ad} between the fiber and particle cluster is needed for long-term stability/storage of the dust layer on fiber. In some sense, U_1, U_2, and the fibers are just "catalysts" and nucleation sites for the fine-grained dusts to agglomerate to reduce their capillary energy. Adhesion is a molecular-scale phenomenon (down to few Å) that depends on both the surface chemistry and fine morphology. It also depends on air moisture and particulate characters. We have already outlined the rational design principles of EAA filter in Section 2.1. Here we would like to reiterate the desirable material properties of the coated fibers. Generally speaking, the antistatic electronic conduction of polymers can be highly nonlinear, that is, a nonlinear electrical I–V relation and non-single exponential dependence of the static charge with time,[33,34] since electronic charge hopping on insulators can require large threshold voltages. So we believe a good fiber/coating combination should have the following materials properties: 1) a suitable nonlinear electronic I–V (antistatic) relation, to improve dust-dust agglomeration after stage-I monopolar charging, 2) robust surface adhesion that is insensitive to moisture below 9.5 g kg^{-1}, so it works consistently in both dry/wet air conditions, 3) a rough surface morphology for increasing dust "sticking probability" by slowing down the particles that do hit, anchoring the dust clusters/layers, and enhancing dust storage capacity, and 4) a large dielectric/pyroelectric/electret response, so it enhances the monopole capture distance $R_{MC}(U_2; q_p)$. We see from our experimental results that $R_{MC}(U_2 = 0; q_p > 0) >> R_C \equiv R_{MC}(U_2 = 0; q_p = 0)$ is the main "trick" for our two-stage EAA device to work, so monopolar charging in stage I is absolutely necessary.

4. Conclusion

In summary, as shown in Figure 5b, we divide the stage-II processes of the EAA coarse filtration into three regions, according to the position of particles.

1) When particles are out of R_{MC}, we call they are in the accelerating region with device-scale (≈10^0 mm). The particles are relatively far away from fibers and cannot distinguish the surface properties of fibers. Therefore, electrostatic force $F_E = q_p E_2$ would drive and accelerate the charged particles towards the fiber surface.
2) When particles are approaching the fiber surfaces within R_{MC}, we call they are in the capture region with fiber-scale (10^1–10^2 µm). Particles in this region would be forced by $F_E = q_p E_{local}$ to hit and get captured by the fiber surface. R_{MC} would depend on q_p, U_2, the fiber material and dielectric/pyroelectric/electret heterogeneity.
3) When particles reach the fiber surfaces, they are in the adhesion region with molecular-scale (≈10^0 Å) distance. In this region, particles may stick to the fiber or resuspend to the air. Filter fibers having reasonable anti-static properties, robust surface adhesion force to dusts and rough surface morphology would hold charged particles firmly, release their charge over a timescale of minutes, and achieve a stably high filtration efficiency in long-term performance.

Therefore, the benefits of coating PDA on PET filter include: 1) the dopamine in situ polymerization process coats the PET fibers with uniform submicron PDA layers, which do not block the airways and thus do not increase the very low air resistance of the PET coarse filter. 2) PDA has a larger dielectric constant, dipole moment, and surface potential than PET, which makes PDA@PET filters show better electrostatic response in the polarizing field of the EAA filtration device. EAA PDA@PET filters would generate a large number of electric dipoles on their surface, and thus capture particles with high electrostatic filtration efficiency. 3) The in situ coated PDA increases the roughness of the PET fiber surfaces and enhances the mechanical filtration efficiency, and then enlarges the surface trap density, strengthens the induced charge accumulation,[62,63] enhancing the particle holding capacity and the electrostatic filtration efficiency.

In all, we developed an EAA PDA@PET filter that possesses enhanced filtration efficiency without increasing the low air resistance of coarse PET filters. Owing to the externally applied electric fields, particles were charged and the PDA@PET fibers were polarized, leading to significantly promoted filtration performance. By controlling the surface microstructure of the filters with an optimized precursor adding amount, the EAA PDA-140@PET filter showed the best performance (highest $QF_{0.3} = 0.553$ Pa^{-1}) among all trials with high $\eta_{0.3}$ of 99.48%, as well as low air resistance of 9.5 Pa at 0.4 m s^{-1} filtration velocity. Compared with the untreated bare PET filter, $p_{0.3}$ was lowered 20× and $QF_{0.3}$ was enhanced by 119%. With the occurrence of pandemic outbreaks such as COVID-19, the role of air purifying technologies became essential to the public. The raw materials of PDA@PET filters in this study are commercially available coarse filters, and the fabrication process of the PDA@PET filters is simple, which is easy to industrialize. Moreover, with its low air resistance (<10 Pa), EAA PDA@PET filter can be directly applied to air supply outlets or the ventilation ducts without adding a driven fan. As Figure S22 (Supporting Information) showed a 284 mm × 200 mm sheet PDA-140@PET filter was constructed, which can be used for building and vehicular ventilation systems.

5. Experimental Section

Preparation of PDA and PDA@PET Filter: Commercial PET fibrous filters (50 mm diameter and 8 mm thickness) were impregnated into 60 mL of 10×10^{-3} M Tris-buffer aqueous solution (pH = 8.5) with stirring for 0.5 h. Different amounts (20, 40, 60, 80, 100, 120, 140, 160, 180, and 200 mg) of dopamine hydrochloride (Sigma-Aldrich, $(HO)_2C_6H_3CH_2CH_2NH_2 \cdot HCl$) were added into the solutions above. In situ polymerization process of dopamine was continued for 24 h with thoroughly stirring. Finally, the PDA@PET filters were obtained after being washed thoroughly by water and ethanol and being dried in an oven at 60 °C for 12 h. Video S1 (Supporting Information) shows the preparation process of a 284 × 200 mm^2 sheet PDA-140@PET filter, which is compatible to large manufacturing.

To obtain pure PDA for characterization, 200 mg dopamine hydrochloride was added into 60 mL of 10×10^{-3} M Tris-buffer aqueous solution (pH = 8.5) with stirring for 24 h. PDA was obtained by centrifuging after being washed thoroughly with water and ethanol, and being dried in an oven at 60 °C for 12 h.

Preparation of PVDF@PET Filter: Firstly, 120 mg PVDF (MTI Corporation, $-(C_2H_2F_2)_n-$) was added into 20 mL N-methyl pyrrolidone (Sigma-Aldrich, C_5H_9NO) and was completely dissolved at 60 °C. Then, the commercial PET filter above was impregnated into the prepared solution for 12 h. Finally, the PVDF@PET filter was obtained after being dried in an oven at 60 °C for 12 h.

EAA Filtration Device: The working principle for the EAA filtration device has been described in the previous studies.[20,23,30] As shown in Figure 1a, in brief, two high voltage power supplies (73030P, Boer Co., Ltd., Suqian, China) work for two stages: stage I is for particle precharging and stage II is for particle and filter polarizing. In the precharging stage, the pin electrode (ELCT2-20A, Fujikura Ltd., Tokyo, Japan) performs corona discharge when supplied with adequate voltage, and charged particles flowing by. In the polarizing stage, the mesh electrodes create an electric field through the filter which is installed between them, and polarize the filter. The gaps between each electrode (the center of the circle-pored metal plate, the tip of the 2 cm length pin electrode, followed by another circle-pored metal plate and 2 metal meshes) are 10, 40, 30, and 20 mm, respectively. The filter clings to the surface of the last mesh electrode. The charging and polarizing voltages were optimally set at +11.5 and +20 kV, respectively, to create strong and safe electric fields.

Filtration Test: The filtration tests were conducted in an acrylic air duct (inner diameter: 50 mm), as shown in Figure 1a. The ambient air was driven through the module after a commercial HEPA filter, which removed ambient particles from airflow, a duct fan (ECMF-100-R, TerraBloom Inc., Chino, USA), a Collison Nebulizer (MRE 6-Jet, BGI Inc., Waltham, USA), which generated feeding particles, a steady flow plate, and the EAA filtration device. For particle generation, 10 wt% KCl solution was used to fill the nebulizer, and used a peristaltic pump (JBT-A, JIHPUMP Co., Ltd., Chongqing, China) to supply 1 L min^{-1} clean air to the nebulizer. In all, KCl aerosol was generated as feeding particles, and the particle size distribution is available in Figure S15 (Supporting Information). The number concentrations of 0.3–10 µm particles were measured by an optical particle counter (Aerotrak 9306, TSI Inc., Shoreview, USA). The concentrations were recorded every 1 min for two times upstream the filter and then two times downstream. The air resistance across the filter was measured by a differential gauge (475-1-FM, Dwyer Instruments, Inc., Michigan, USA). The air temperature, relative humidity, and filtration velocity were measured by a thermo-anemometer (Extech 45158, FLIR Systems Inc., Nashua, USA) at the air duct exhaust. The supplying voltages and the loop currents of the charging and polarizing zones were recorded by their corresponding power supplies.

Characterization: Fourier-transform infrared (FT-IR) spectrometer (Bruker Vertex70 instrument) of all the samples was performed in the wave-number range 400–4000 cm^{-1}. X-ray diffraction (XRD) was conducted using a Bruker D8 Advance diffractometer in an angle range of 10–80° (2θ) using Cu Kα radiation (λ = 1.5418 Å). The morphologies of the fibbers were investigated by using a field emission scanning electron microscope (SEM, Hitachi S4800) coupled with energy dispersive X-ray spectra (EDS). Thermogravimetric analysis (TGA) and differential thermal gravimetric analysis (DTA) were conducted on a NETZSCH STA449F3 thermal analyzer from room temperature to 600 °C at a heating rate of 5 °C min^{-1} in N_2 atmosphere. The PDA films were pressed into pellets under a pressure of 20 MPa to obtain the topography and surface potential map by using an atomic force microscope (AFM, Bruker DIMENSION ICON). The relative dielectric constants of the materials were obtained by using a precision impedance analyzer (Agilent 4294A, Agilent Technologies, Inc.) and the detailed process was shown in Supporting Information.

Simulation: The theoretical dipole moments and molecular electrostatic potential of the single molecules were calculated by the ground-state density functional theory (DFT) using B3LYP hybrid functionals with 6-31G basis set incorporated in the Gaussian 03 program.[64]

Supporting Information

Supporting Information is available from the Wiley Online Library or from the author.

Acknowledgements

The research was supported by the National Natural Science Foundation of China (nos. 52078269 and 51521005). E.T. thanks the support provided by the China Scholarship Council (CSC) (no. 201906210128) during a visit to the Massachusetts Institute of Technology, and Kai Liu in Tsinghua University for helping prepare samples for the dielectric constant test. The Testing Technology Center of Materials and Devices (Tsinghua Shenzhen International Graduate School, SIGS) was also gratefully acknowledged. The authors acknowledge support by Yintai Investment Co. LLC.

Conflict of Interest

The authors declare no conflict of interest.

Data Availability Statement

The data that supports the findings of this study are available in the supplementary material of this article.

Keywords

adhesion, antistatic, long-term accumulation, monopole capture, particulate matter

Received: April 7, 2021
Revised: June 17, 2021
Published online: July 26, 2021

[1] G. Grande, P. L. S. Ljungman, K. Eneroth, T. Bellander, D. Rizzuto, *JAMA Neurol.* **2020**, *77*, 801.
[2] S. Feng, D. Gao, F. Liao, F. Zhou, X. Wang, *Ecotoxicol. Environ. Saf.* **2016**, *128*, 67.
[3] M. Loxham, D. E. Davies, S. T. Holgate, *Br. Med. J.* **2019**, *367*, l6609.
[4] M. G. Zhou, H. D. Wang, X. Y. Zeng, P. Yin, J. Zhu, W. Q. Chen, X. H. Li, L. J. Wang, L. M. Wang, Y. N. Liu, J. M. Liu, M. Zhang, J. L. Qi, S. C. Yu, A. Afshin, E. Gakidou, S. Glenn, V. S. Krish, M. K. Miller-Petrie, W. C. Mountjoy-Venning, E. C. Mullany, S. B. Redford, H. Y. Liu, M. Naghavi, S. I. Hay, L. H. Wang, C. J. L. Murray, X. F. Liang, *Lancet* **2019**, *394*, 1145.
[5] The United States Environmental Protection Agency, *Exposure Factors Handbook*, Office of Research and Development, Washington, USA **1997**.
[6] T. L. Xia, Y. Bian, L. Zhang, C. Chen, *Energy Build.* **2018**, *158*, 987.
[7] C. Liu, P.-C. Hsu, H.-W. Lee, M. Ye, G. Zheng, N. Liu, W. Li, Y. Cui, *Nat. Commun.* **2015**, *6*, 6205.
[8] S. Wang, X. Zhao, X. Yin, J. Yu, B. Ding, *ACS Appl. Mater. Interfaces* **2016**, *8*, 23985.
[9] G.-H. Zhang, Q.-H. Zhu, L. Zhang, F. Yong, Z. Zhang, S.-L. Wang, Y. Wang, L. He, G.-H. Tao, *Nat. Commun.* **2020**, *11*, 1653.
[10] H. Liu, S. C. Zhang, L. F. Liu, J. Y. Yu, B. Ding, *Adv. Funct. Mater.* **2020**, *30*, 1909554.
[11] A. Al Rai, E. Stojanovska, G. Fidan, E. Yetgin, Y. Polat, A. Kilic, A. Demir, S. Yilmaz, *Polym. Eng. Sci.* **2020**, *60*, 1186.
[12] B. Maze, H. V. Tafreshi, Q. Wang, B. Pourdeyhimi, *J. Aerosol Sci.* **2007**, *38*, 550.
[13] X. Q. Li, N. Wang, G. Fan, J. Y. Yu, J. Gao, G. Sun, B. Ding, *J. Colloid Interface Sci.* **2015**, *439*, 12.
[14] R. F. Zhang, C. Liu, P. C. Hsu, C. F. Zhang, N. Liu, J. S. Zhang, H. R. Lee, Y. Y. Lu, Y. C. Qiu, S. Chu, Y. Cui, *Nano Lett.* **2016**, *16*, 3642.
[15] Y. Bai, C. B. Han, C. He, G. Q. Gu, J. H. Nie, J. J. Shao, T. X. Xiao, C. R. Deng, Z. L. Wang, *Adv. Funct. Mater.* **2018**, *28*, 1706680.
[16] N. Bhardwaj, S. C. Kundu, *Biotechnol. Adv.* **2010**, *28*, 325.
[17] S. Jung, J. Kim, *Polymers* **2020**, *12*, 1714.
[18] P. C. Raynor, B. G. Kim, G. Ramachandran, M. R. Strommen, J. H. Horns, A. J. Streifel, *Indoor Air* **2008**, *18*, 51.
[19] E. Tian, Y. Gao, J. Mo, *Build. Environ.* **2019**, *164*, 106348.
[20] E. Tian, J. Mo, *Energy Build.* **2019**, *186*, 276.
[21] B. Shi, L. Ekberg, *Environ. Sci. Technol.* **2015**, *49*, 6891.
[22] Z. B. Feng, Z. W. Long, T. Yu, *J. Electrost.* **2016**, *83*, 52.
[23] E. Tian, J. Mo, Z. Long, H. Luo, Y. Zhang, *Build. Environ.* **2018**, *135*, 153.
[24] C. X. Li, S. Y. Kuang, Y. H. Chen, Z. L. Wang, C. Li, G. Zhu, *ACS Appl. Mater. Interfaces* **2018**, *10*, 24332.
[25] D. Y. Choi, E. J. An, S. H. Jung, D. K. Song, Y. S. Oh, H. W. Lee, H. M. Lee, *Sci. Rep.* **2018**, *8*, 5747.
[26] D. Y. Choi, S. H. Jung, D. K. Song, E. J. An, D. Park, T. O. Kim, J. H. Jung, H. M. Lee, *ACS Appl. Mater. Interfaces* **2017**, *9*, 16495.
[27] G. Q. Gu, C. B. Han, C. X. Lu, C. He, T. Jiang, Z. L. Gao, C. J. Li, Z. L. Wang, *ACS Nano* **2017**, *11*, 6211.
[28] G. Q. Gu, C. B. Han, J. J. Tian, T. Jiang, C. He, C. X. Lu, Y. Bai, J. H. Nie, Z. Li, Z. L. Wang, *Nano Res.* **2018**, *11*, 4090.
[29] G. Liu, J. Nie, C. Han, T. Jiang, Z. Yang, Y. Pang, L. Xu, T. Guo, T. Bu, C. Zhang, Z. L. Wang, *ACS Appl. Mater. Interfaces* **2018**, *10*, 7126.
[30] E. Tian, F. Xia, J. Wu, Y. Zhang, J. Li, H. Wang, J. Mo, *ACS Appl. Mater. Interfaces* **2020**, *12*, 29383.
[31] Z. Wang, Y. Cheng, M. Yang, J. Huang, D. Cao, S. Chen, Q. Xie, W. Lou, H. Wu, Composites, Part B **2018**, *140*, 83.
[32] Hollingsworth and Vose, Technical data for HVAC filters, http://www.hollingsworth-vose.com/en/Products/Filtration-Media/Air-Filtration1/HVAC-filtration (accessed: Feburary 2020).
[33] V. E. Shashoua, *J. Polym. Sci.* **1958**, *33*, 65.
[34] B. Górnicka, M. Mazur, K. Sieradzka, E. Prociów, M. Lapinski, *Acta Phys. Pol., A* **2010**, *117*, 869.
[35] S. Roh, K. Park, J. Kim, *Polymers* **2019**, *11*, 1822.
[36] Z. Wang, C. Zhao, Z. Pan, *J. Colloid Interface Sci.* **2015**, *441*, 121.
[37] H. Gao, Y. Yang, O. Akampumuza, J. Hou, H. Zhang, X. Qin, *Environ. Sci. Nano* **2017**, *4*, 864.
[38] D. Lv, R. Wang, G. Tang, Z. Mou, J. Lei, J. Han, S. De Smedt, R. Xiong, C. Huang, *ACS Appl. Mater. Interfaces* **2019**, *11*, 12880.
[39] B. Khalid, X. Bai, H. Wei, Y. Huang, H. Wu, Y. Cui, *Nano Lett.* **2017**, *17*, 1140.
[40] D. Wang, K. Wang, L. Sun, H. Wu, J. Wang, Y. Zhao, L. Yan, Y. Luo, K. Jiang, Q. Li, S. Fan, J. Li, J. Wang, *Carbon* **2018**, *139*, 145.
[41] C. W. Xu, W. X. Xie, X. D. Si, J. Zhang, J. G. Yang, *Environ. Res.* **2018**, *166*, 167.
[42] Q.-Y. Chen, C.-X. Li, T. Wei, H.-B. Sun, S.-L. Zhang, X.-T. Luo, G.-J. Yang, C.-J. Li, M.-L. Liu, *RSC Adv.* **2015**, *5*, 102126.
[43] H. Dislich, E. Hussmann, *Thin Solid Films* **1981**, *77*, 129.
[44] Q. Sun, W. W.-F. Leung, *Sep. Purif. Technol.* **2020**, *240*, 116606.
[45] H. Lee, S. M. Dellatore, W. M. Miller, P. B. Messersmith, *Science* **2007**, *318*, 426.
[46] Z. D. Wang, M. M. Yang, Y. H. Cheng, J. Y. Liu, B. Xiao, S. Y. Chen, J. L. Huang, Q. Xie, G. L. Wu, H. J. Wu, *Composites, Part A* **2019**, *118*, 302.
[47] Y. L. Liu, K. L. Ai, L. H. Lu, *Chem. Rev.* **2014**, *114*, 5057.
[48] W. X. Cheng, F. F. Fan, Y. Zhang, Z. C. Pei, W. J. Wang, Y. X. Pei, *Polymers* **2017**, *9*, 135.
[49] R. Bhunia, A. Yadav, S. Jha, D. Bhattacharyya, S. Hussain, R. Bhar, A. Pal, *Polymer* **2015**, *78*, 1.
[50] Y. Wang, Q. Qu, S. Gao, G. Tang, K. Liu, S. He, C. Huang, *Carbon* **2019**, *155*, 706.

[51] K. W. Lee, B. Y. H. Liu, *J. Air Pollut. Control Assoc.* **1980**, *30*, 377.
[52] Y. Liu, Z. Ning, Y. Chen, M. Guo, Y. Liu, N. K. Gali, L. Sun, Y. Duan, J. Cai, D. Westerdahl, X. Liu, K. Xu, K.-f. Ho, H. Kan, Q. Fu, K. Lan, *Nature* **2020**, *582*, 557.
[53] S. Bourrous, L. Bouilloux, F. X. Ouf, P. Lemaitre, P. Nerisson, D. Thomas, J. C. Appert-Collin, *Powder Technol.* **2016**, *289*, 109.
[54] R. Ravichandran, A. X. Wang, J. F. Wager, *Opt. Mater.* **2016**, *60*, 181.
[55] P. Hervé, L. K. J. Vandamme, *Infrared Phys. Technol.* **1994**, *35*, 609.
[56] J. Lee, J. Kim, *Polymers* **2020**, *12*, 721.
[57] P. Jiang, X. Zhao, Y. Li, Y. Liao, T. Hua, X. Yin, J. Yu, B. Ding, *Compos. Commun.* **2017**, *6*, 34.
[58] X. Zhao, Y. Li, T. Hua, P. Jiang, X. Yin, J. Yu, B. Ding, *ACS Appl. Mater. Interfaces* **2017**, *9*, 12054.
[59] H. L. Schreuder-Gibson, P. Gibson, P. Tsai, *Int. Nonwovens J.* **2004**, *os-13*, 1558925004os-13.
[60] H.-J. Choi, E.-S. Park, J.-U. Kim, S. H. Kim, M.-H. Lee, *Aerosol Sci. Technol.* **2015**, *49*, 977.
[61] R. R. Cai, L. Z. Zhang, A. B. Bao, *Build. Environ.* **2018**, *131*, 210.
[62] C. Y. Li, J. L. He, J. Hu, *IEEE Trans. Dielectr. Electr. Insul.* **2016**, *23*, 3071.
[63] T. Vu-Cong, L. Zavattoni, P. Vinson, A. Girodet, presented at 2016 IEEE CEIDP, Toronto, Canada, October **2016**.
[64] M. J. Frisch, G. W. Trucks, H. B. Schlegel, G. E. Scuseria, M. A. Robb, J. R. Cheeseman, J. A. Montgomery Jr., T. Vrevon, K. N. Kudin, J. C. Bur-ant, J. M. Millam, S. S. Iyengar, J. Tomasi, V. Barone, B. Menucci, M. Cossi, G. Scalmani, N. Rega, G. A. Petersson, H. Nakatsuji, M. Hada, M. Ehara, K. Toyota, R. Fukuda, J. Hasegawa, M. Ishida, T. Nakajima, Y. Honda, O. Kitao, H. Nakai, M. Klene, X. Li, J. E. Knox, H. P. Hratchian, J. B. Cross, C. Adamo, J. Jaramillo, R. Gomparts, R. E. Stratmann, O. Yazyev, A. J. Austin, R. Cammi, C. Pomelli, J. W. Ochterski, P. Y. Ayala, K. Morokuma, G. A. Voth, P. Salvador, J. J. Dannenberg, V. G. Zakrzew-ski, S. Dapprich, A. D. Daniels, M. C. Strain, O. Farkas, D. K. Malick, A. D. Rabuck, K. Raghavachari, J. B. Foresman, J. V. Ortiz, Q. Cui, A. G. Baboul, S. Clifford, J. Cioslowski, B. B. Stefanov, G. Liu, A. Liashenko, P. Piskorz, I. Komaromi, R. L. Martin, D. J. Fox, T. Keith, M. A. Al-Laham, A. A. Al-Laham, Peng, A. Namayakkara, M. Challacombe, P. M. W. Gill, B. Johnson, W. Chen, M. Wong, C. Gonzalez, J. A. Pople, Gaussian 03, E.01, Gaussian, Inc., Wallingford, CT, **2004**.

NANO MICRO small

Supporting Information

for *Small,* DOI: 10.1002/smll.202102051

Ultralow Resistance Two-Stage Electrostatically Assisted Air Filtration by Polydopamine Coated PET Coarse Filter

Enze Tian, Qipeng Yu, Yilun Gao, Hua Wang, Chao Wang, Yinping Zhang, Baohua Li, Meifang Zhu, Jinhan Mo, Guiyin Xu,* and Ju Li**

Supporting Information

Ultralow resistance two-stage electrostatically assisted air filtration by polydopamine coated PET coarse filter

Enze Tian, Qipeng Yu, Yilun Gao, Hua Wang, Chao Wang, Yinping Zhang, Baohua Li, Meifang Zhu, Jinhan Mo, Guiyin Xu*, and Ju Li**

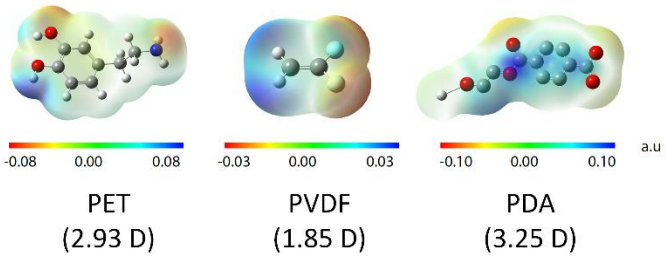

Figure S1. Molecular models of different polymers including PET, PVDF and PDA with calculated dipole moments of the repeating unit of each polymer.

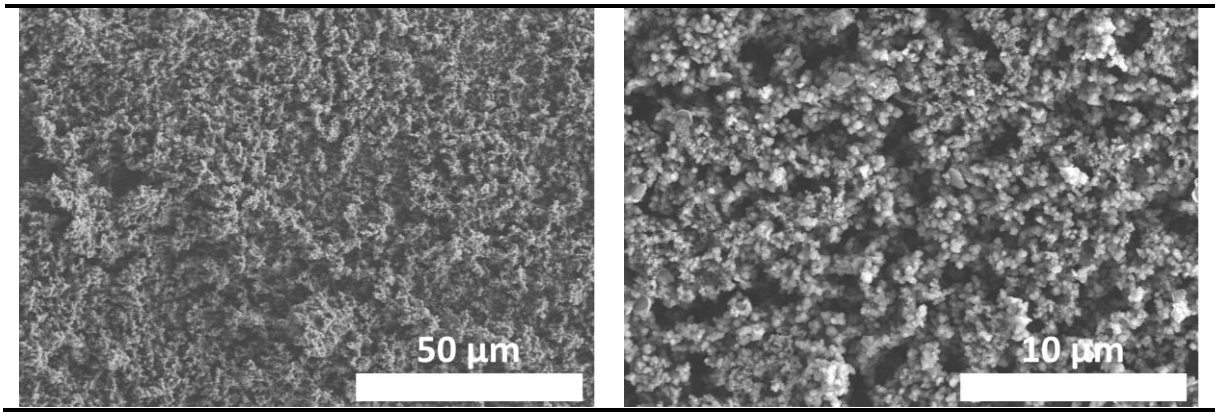

Figure S2. SEM images of pure PDA.

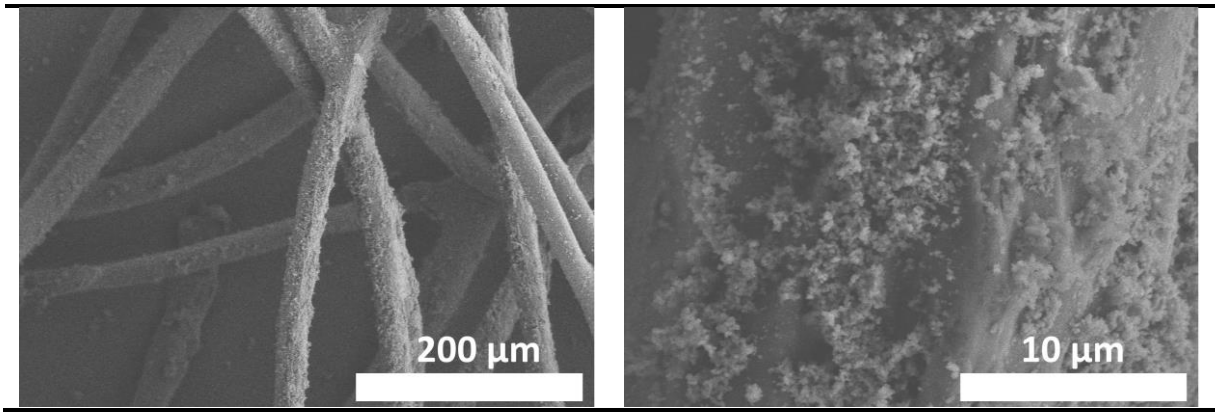

Figure S3. SEM images of PDA-140@PET filter.

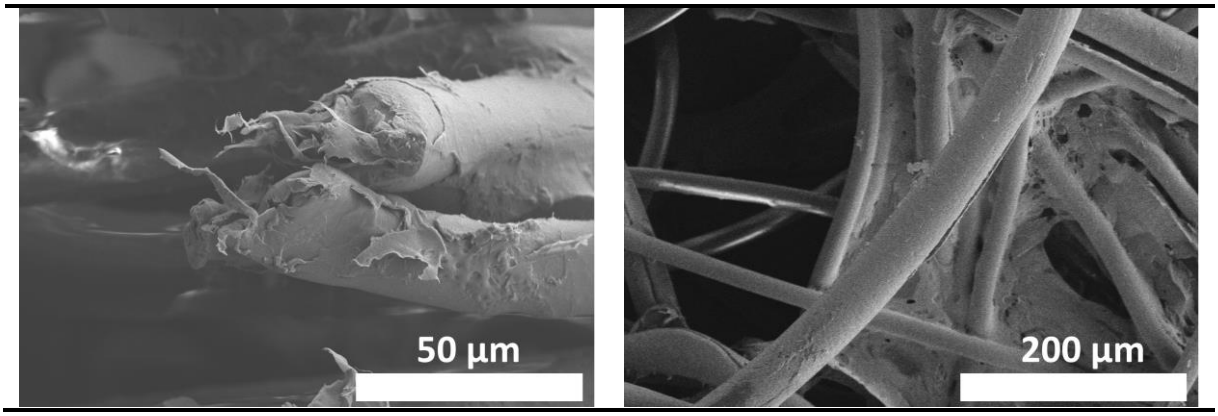

Figure S4. SEM images of PVDF-120@PET filter.

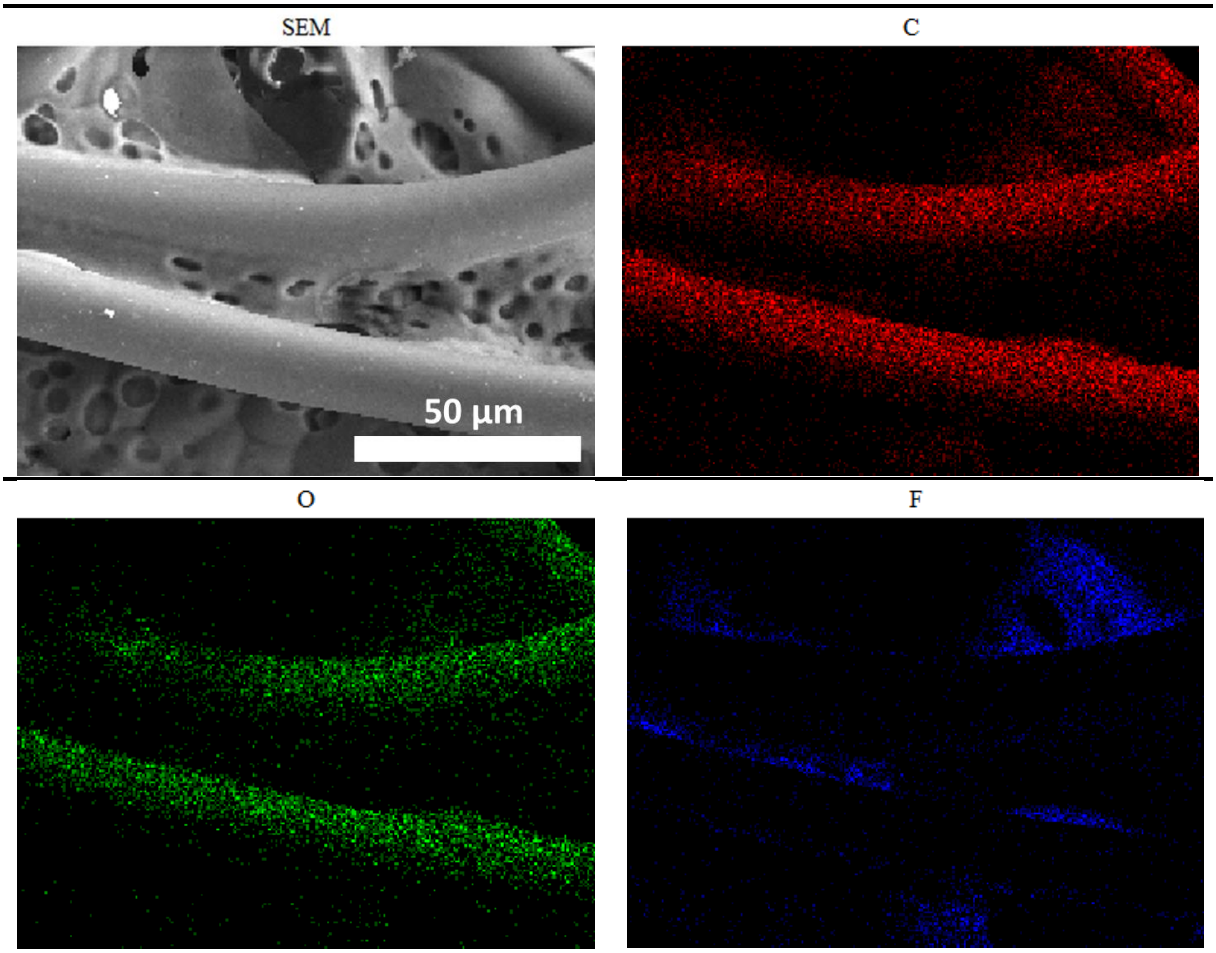

Figure S5. SEM image and corresponding EDS mapping images of PVDF-120@PET filter.

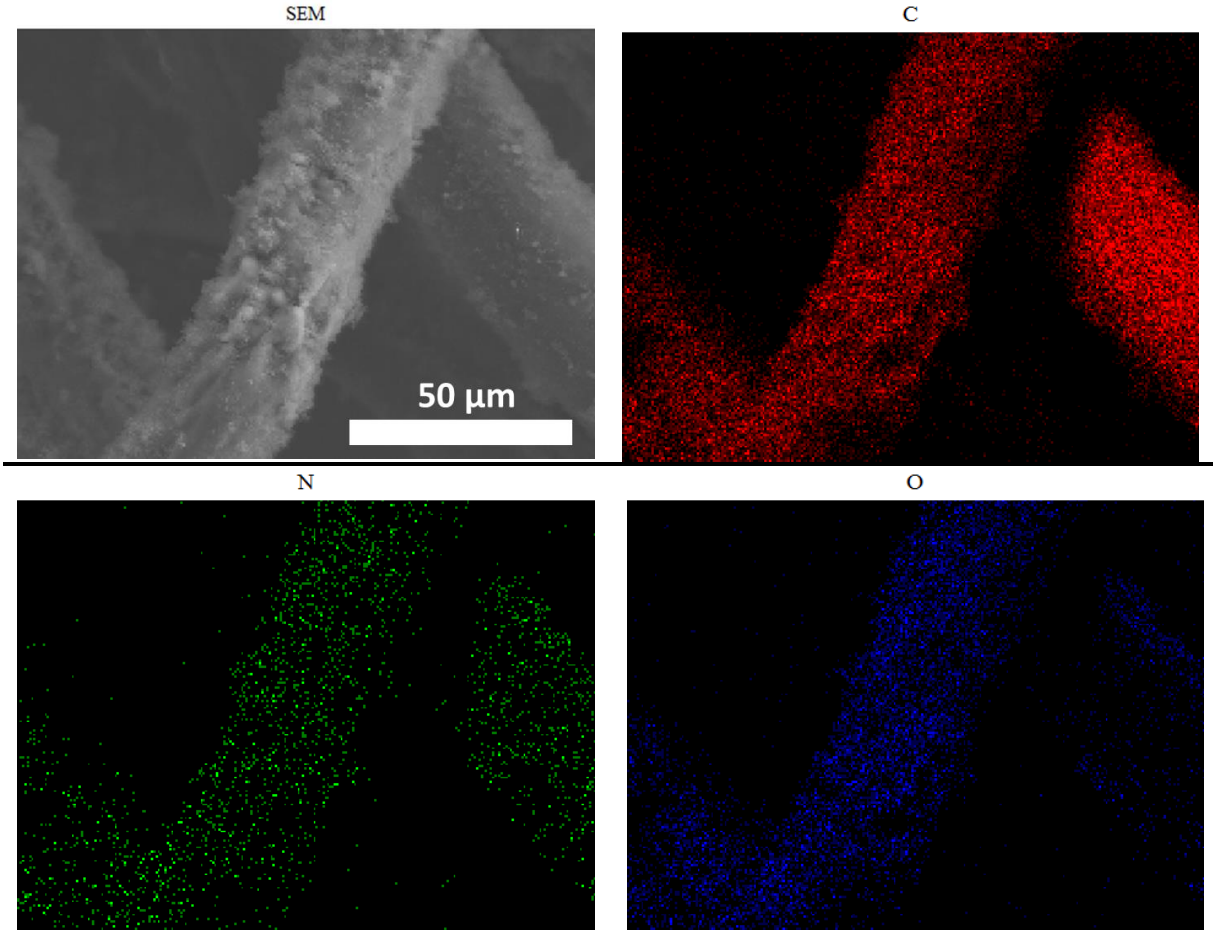

Figure S6. SEM image and corresponding EDS mapping images of PDA-120@PET filter.

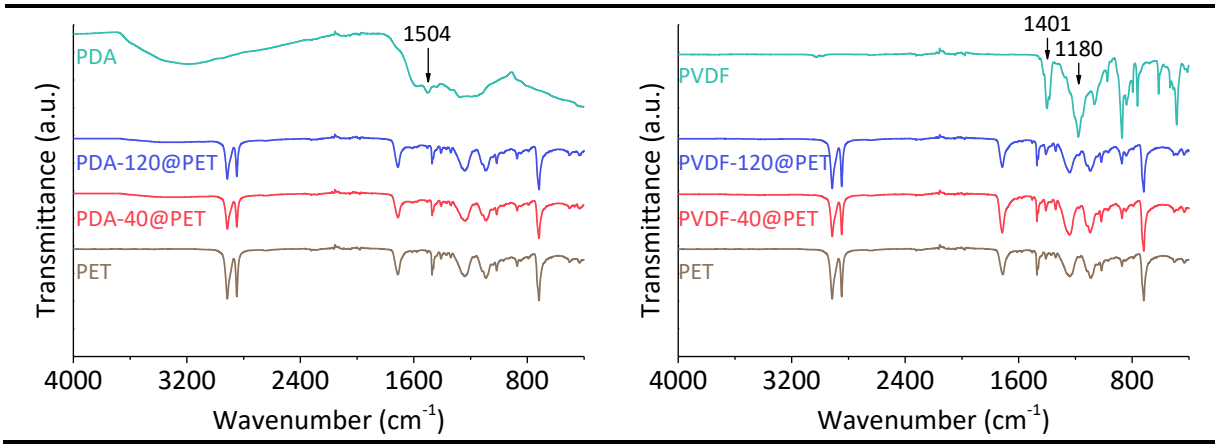

Figure S7. FTIR spectra of the bare PET filter, PDA@PET and PVDF@PET filters with different precursor adding amount, and pure PDA and PVDF.

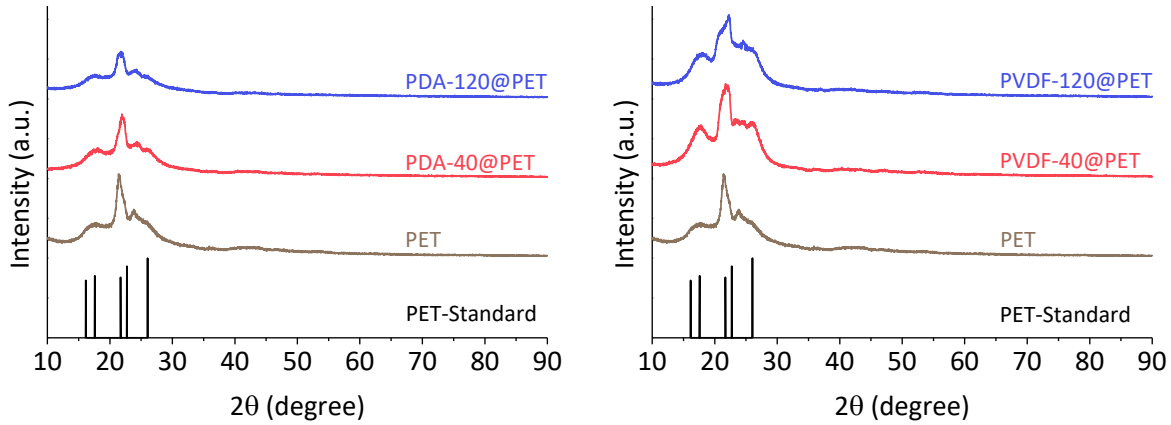

Figure S8. XRD patterns of the standard crystalline PET, bare PET filter, PDA@PET and PVDF@PET filters with different precursor adding amount.

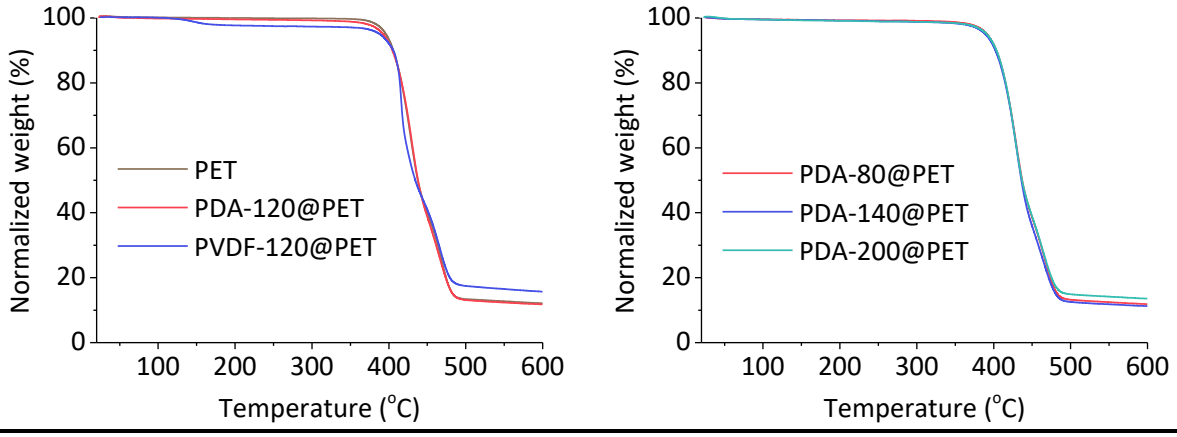

Figure S9. TGA curves of the bare PET filter, PVDF-120@PET filter, and PDA@PET filters with different precursor adding amount.

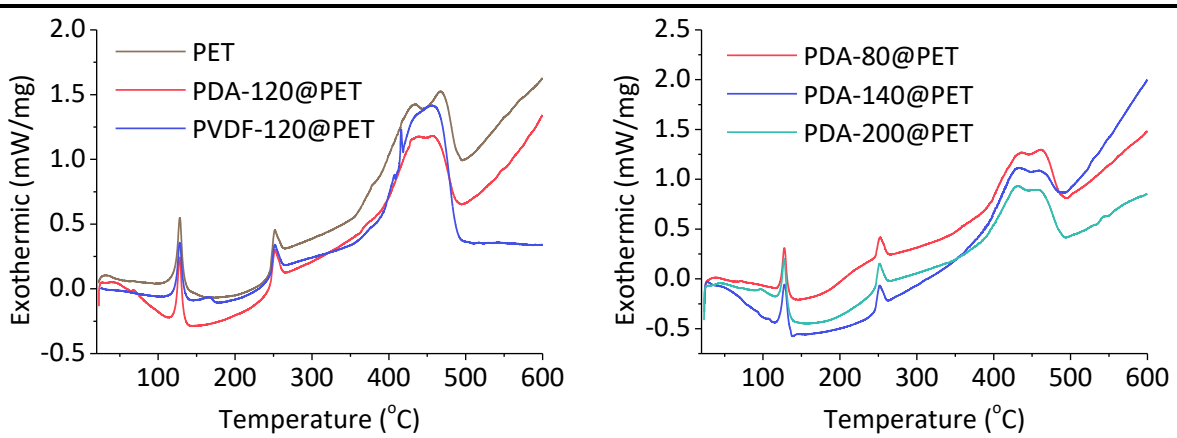

Figure S10. DSC curves of the bare PET filter, PVDF-120@PET filter, and PDA@PET filters with different precursor adding amount.

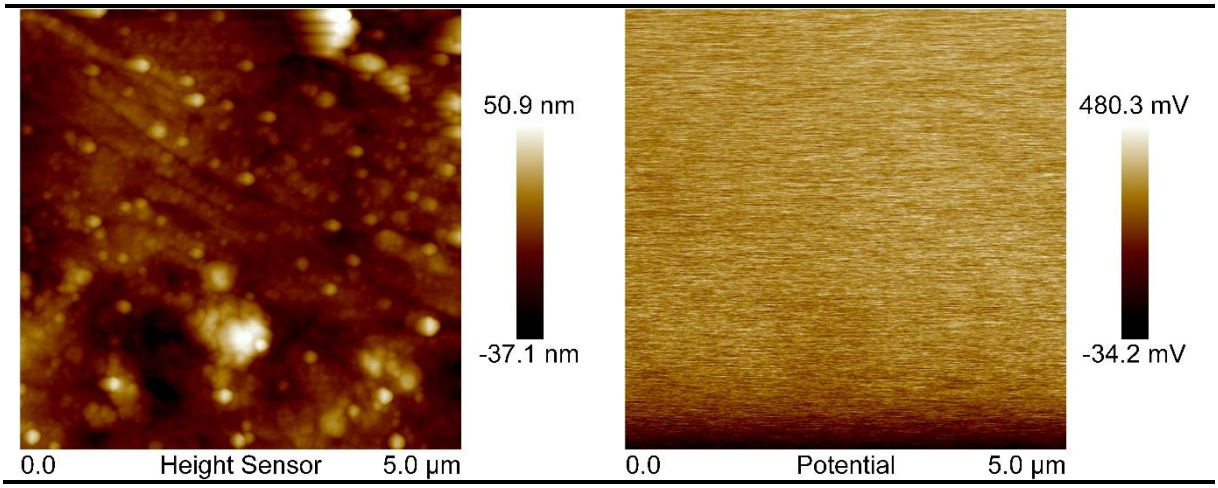

Figure S11. AFM topography (left) and surface potential map (right) of bare PET filter.

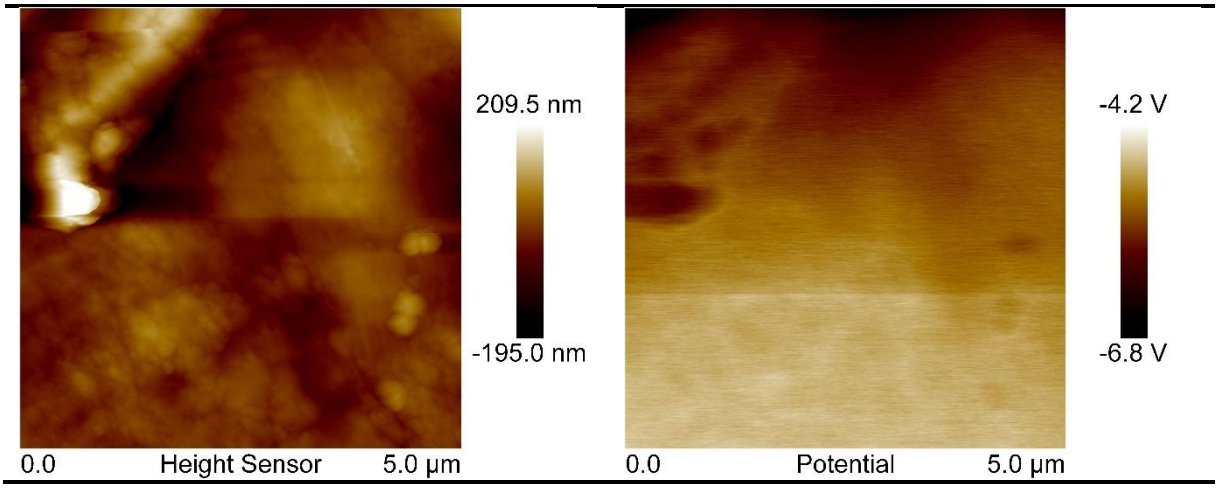

Figure S12. AFM topography (left) and surface potential map (right) of PDA-140@PET filter.

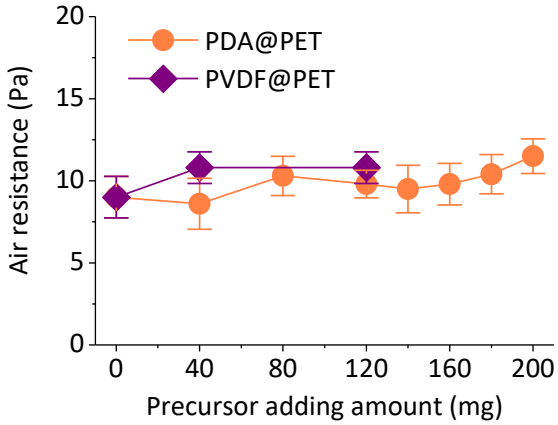

Figure S13. Air resistances of PVDF@PET and PDA@PET filters with different precursor adding amount.

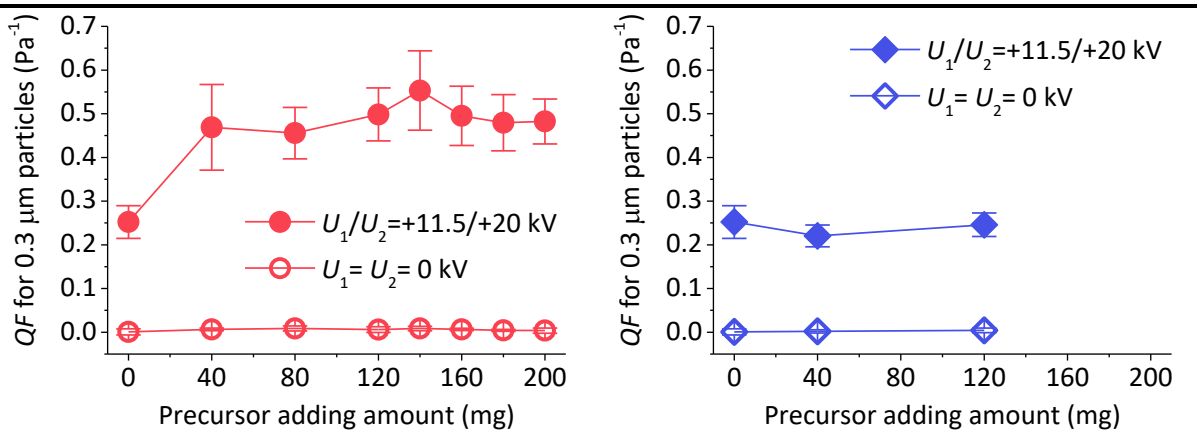

Figure S14. $QF_{0.3}$ (quality factors for 0.3 μm particles) of PDA@PET (left) and PVDF@PET (right) filters with different precursor adding amount and U_1, U_2 being turned on or off.

Table S1

Information and performance of the commercial HVAC filters (U_1 = U_2 = 0).

Model	Single-pass filtration efficiency for 0.3 μm particles (%)	Air resistance (Pa)	Filtration velocity (m s^{-1})	Equivalent air resistance at 0.4 m s^{-1} (Pa)
HE15731A	75	64	0.053	483.0
HE14731A	61	44	0.053	332.1
HF13731A	48	34	0.053	256.6
HE15732A	74	64	0.053	483.0
HE14732A	61	44	0.053	332.1
HF13732A	48	34	0.053	256.6
HF13931A	50	26	0.053	196.2
HE14931A	60	31	0.053	234.0
HE9799	95	115	0.053	867.9
HE9699	88	88	0.053	664.2
HE9599S	75	63	0.053	475.5
HE9195S	65	45	0.053	339.6
HF8185S	50	30	0.053	226.4
HF6165S	25	11	0.053	83.0
HD2433	95	135	0.053	1018.9
HE1613	95	135	0.053	1018.9
HE1513	75	65	0.053	490.6
HE1413	66	55	0.053	415.1
HF0712	25	14	0.053	105.7
PSS1631A	96.5	17	0.053	125.7
PSS1531A	90	12	0.053	88.8
PSS1331A	85	11	0.053	81.4
PSS1131A	78	9	0.053	66.6
AS9030SS	93.7	22	0.053	162.7
AS8030SS	90	15	0.053	110.9
AS6030SS	68	6	0.053	44.4
AS4030SS	59	3	0.053	22.2
AS9520DD-H	93.4	91	0.11	330.9
AS9020DD-H	89	75	0.11	272.7
AS8020DD-H	89	75	0.11	272.7
AS6020DD-H	63	26	0.11	94.5
AS9030SS-H	87	75	0.11	272.7
AS8030SS-H	77	48	0.11	174.5
AS6030SS-H	60	21	0.11	76.4
AS4030SS-H	45	19	0.11	69.1

AS779/35B-H	25	65	0.11	236.4

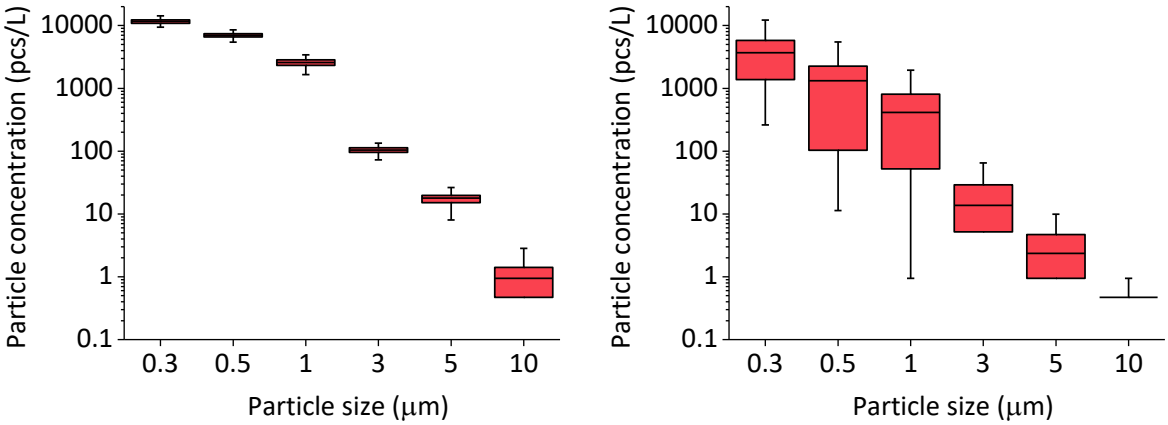

(a) Initial performance tests (b) Long-term performance test for PDA-140@PET filter

Figure S15. Size distribution of loading particles during the tests.

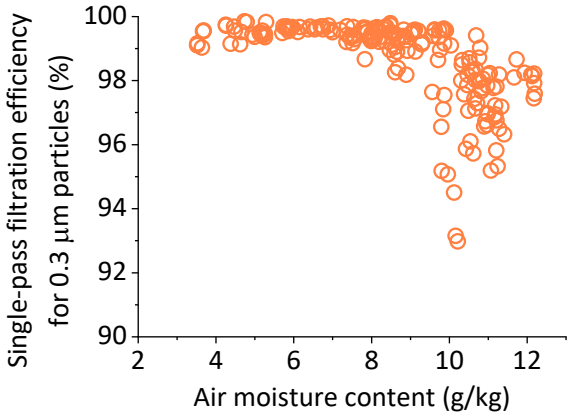

Figure S16. Relationship between sing-pass filtration efficiency for 0.3 μm particles and air moisture content. Data were extracted from the long-term performance of EAA PDA-140@PET filter.

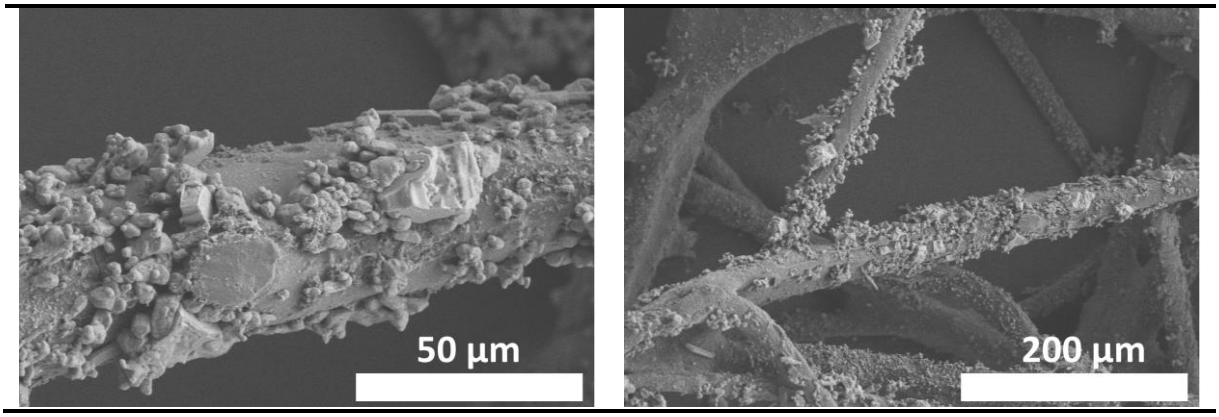

Figure S17. SEM images of KCl particles captured by EAA PDA-140@PET filter.

Table S2
Environmental and operating parameters during the long-term performance test. Accumulated PM_{10} amount was calculated by the method shown below. Charging voltage U_1 controlled at +12 kV, and polarizing voltage U_2 was controlled at +20 kV, respectively. The polarizing current maintained zero during the whole testing period.

Day	Air temperature (ºC)	Air relative humidity (%)	Accumulated PM_{10} amount ($g\ m^{-2}$)	Charging current (μA)
1	23.5-24.8	36.0-40.9	0.832	4-7
2	23.5-24.7	27.1-43.5	2.09	5-7
3	24.5-25.2	21.5-26.8	4.65	7-8
4	23.6-24.3	39.5-45.9	5.55	3-7
5	23.4-24.2	45.6-53.2	6.28	5-6
6	23.1-24.2	58.2-62.1	6.40	2-6
7	23.6-24.4	63.6-66.5	6.50	6-7
8	22.0-23.0	47.8-52.4	8.06	5-8
9	22.1-24.5	23.6-37.3	9.42	6-8
10	23.8-24.7	18.9-23.3	11.7	5-7
11	23.8-24.7	27.3-34.7	13.7	3-8
12	23.9-25.1	42.9-53.7	15.0	4-5
13	23.6-24.2	42.1-52.1	16.2	2-12
14	23.4-24.2	54.8-61.5	16.4	4-12
15	22.8-23.9	46.1-65.0	16.4	6-9
16	22.8-23.8	43.8-48.7	17.7	6-9
17	23.4-24.4	31.1-33.0	19.9	8-9
18	23.4-24.1	35.1-40.0	22.3	8-9
19	23.6-24.3	43.5-50.7	23.1	7-8
20	23.5-24.3	56.1-61.5	23.2	6-8
21	23.2-23.9	41.5-52.4	24.1	6-8
22	23.7-24.4	41.0-44.3	25.7	7-9
23	23.4-24.2	51.7-54.3	26.6	6-8
24	23.7-24.7	54.9-58.8	26.7	6-8
25	23.9-24.8	55.2-58.1	26.8	2-8
26	23.7-24.6	56.2-60.0	26.8	3-9
27	23.9-24.6	53.6-57.2	27.2	6-8
28	23.3-23.9	46.6-51.6	28.7	6-8
29	23.1-24.1	54.5-57.2	28.8	5-8
30	22.5-23.4	53.3-56.5	28.9	7-8

Table S3
The long-term performance comparison of EAA PDA-140@PET filters and the commercial pleated electret filters for 240-hour running.

	EAA PDA-140@PET filter	Commercial electret filter[1]
Original $\eta_{0.3}$	99.34%	99.52%
Original $\eta_{0.5}$	99.48%	99.51%
Original η_1	99.83%	99.41%
Original air resistance	9.5 Pa	59.8 Pa
Average $\eta_{0.3}$	98.63%	90.06%
Average $\eta_{0.5}$	99.04%	91.11%
Average η_1	99.83%	92.83%
Final air resistance	17.4 Pa	98.4 Pa

Note: the face air velocities for the EAA PDA-140@PET filter and the electret filter were 0.4 and 1.0 $m\ s^{-1}$, respectively.

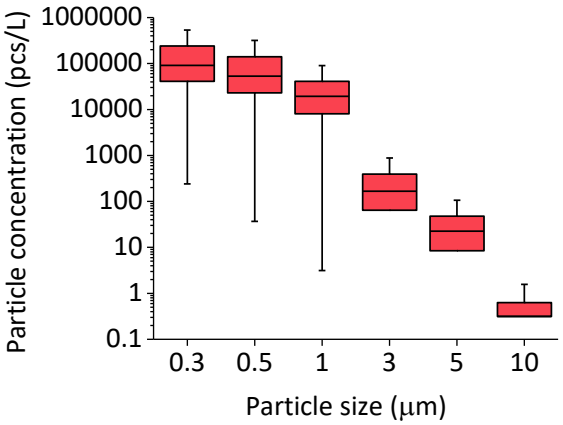

Figure S18. Size distribution of loading particles during the long-term performance test for PDA-20@PET and PDA-200@PET filters.

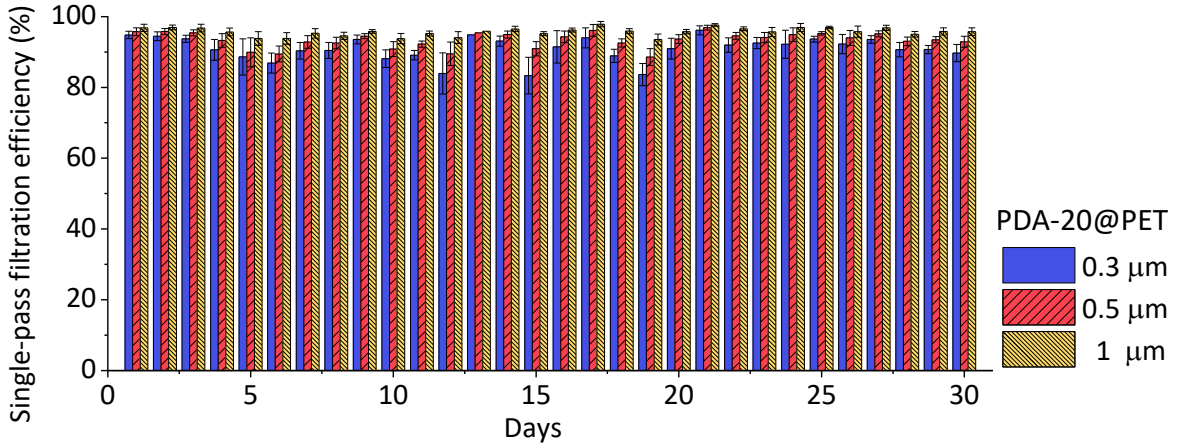

Figure S19. Long-term single pass filtration efficiencies of EAA PDA-20@PET filter for 0.3-1 μm particles. The error bars are the standard deviations of 40 observations of the experiments in each day.

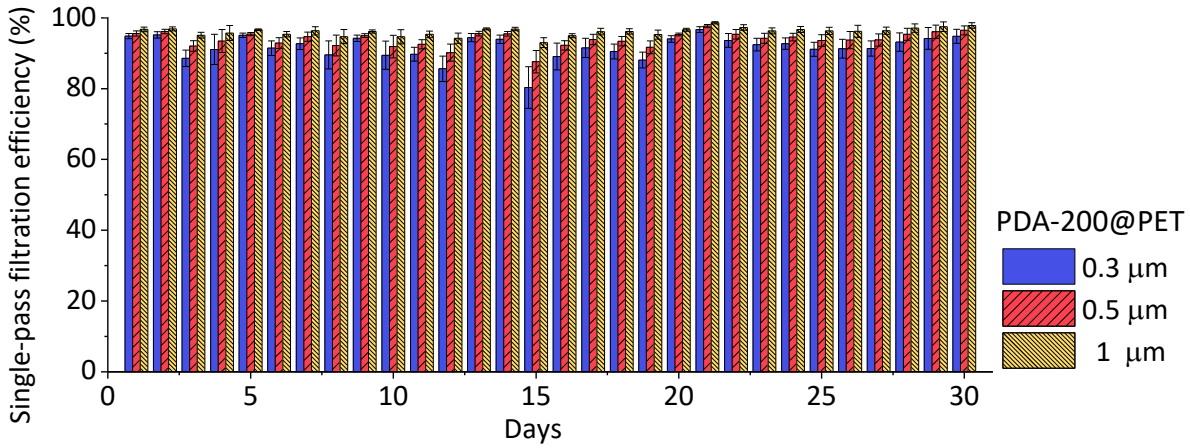

Figure S20. Long-term single pass filtration efficiencies of EAA PDA-200@PET filter for 0.3-1 μm particles. The error bars are the standard deviations of 40 observations of the experiments in each day.

(a) Clean surfaces (b) Dirty (particle covered) surfaces

Figure S21. Photos of charging pins before and after 30-day running.

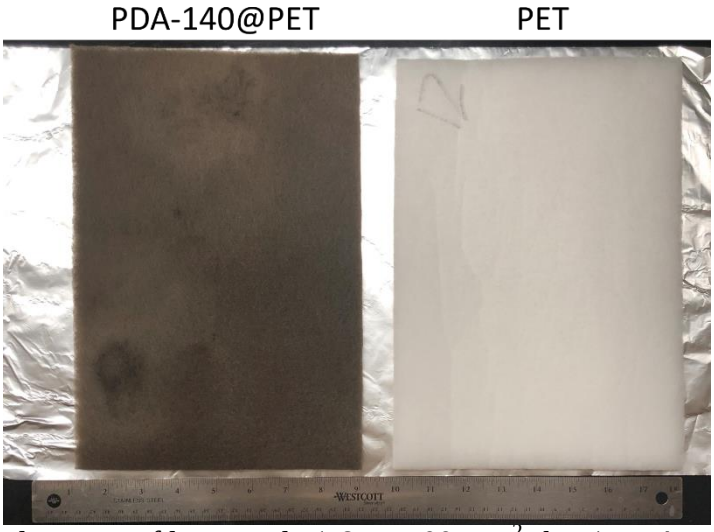

Figure S22. Digital images of large scale (284 × 200 mm^2 sheet) PDA-140@PET and bare PET filters.

Video S1 (separate file). Preparation process of the PDA-140@PET filter compatible to large manufacturing.

Methods for calculating accumulated PM_{10} amount (M_{acc}, g m^{-2})

Accumulated PM_{10} amounts (M_{acc}, g m^{-2}) were approximately estimated by the similar method in previous study[1]:

$$M_{\text{acc},\,n} = \sum_{d=1}^{n} M_{\text{daily},\,d} \qquad \text{(S1)}$$

$$M_{\text{daily},\,d} = 10^{-8}\pi\frac{\rho v_{\text{air}}}{Q_{\text{s}}}\cdot\sum_{t=0}^{480}\sum_{i=1}^{6}\left[C_{\text{up},\,t}\left(d_{\text{p},i}\right)\cdot\eta_t\left(d_{\text{p},i}\right)\cdot d_{\text{p},i}^{3}\right] \qquad \text{(S2)}$$

where $M_{acc,n}$ is accumulated PM_{10} amount after n day(s), g m^{-2}; $M_{daily,d}$ is PM_{10} daily collecting amount in the d^{th} day, g m^{-2}; ρ is the density of KCl particles, 1.99 g cm^{-3}; v_{air} is the air velocity in the testing air duct, m s^{-1}; Q_s is the sampling air amount of the particle counter per minute, 2.1225 L; t is the time in a day, minute; $d_{p,i=1\text{-}6}$ represent particle sizes of 0.3, 0.5, 1, 3, 5, and 10 μm, respectively.

Methods for measuring relative dielectric constant (ε_r)

The relative dielectric constant (ε_r) of the materials can be obtained by the following process:

Sample preparation. Filters were compressed into membranes, PDA and PVDF powders were compressed into tablets using a manual hydraulic machine. The operating pressure was controlled at 12 Mpa and 20 Mpa for filters and powders, respectively. All samples were compressed tightly with a diameter of 10 mm.

Dielectric properties measurement. The capacitance (C) of the sample between the two circular electrodes was measured by a precision impedance analyzer (Agilent 4294A, Agilent Technologies, Inc). The relative dielectric constant, ε_r, was then calculated by:

$$\varepsilon_r = \frac{4C\delta}{\varepsilon_0 \pi d^2} \quad \text{(S3)}$$

where C is the capacitance of the sample at 1.0 MHz, F; δ is the thickness of the compressed sample, m; ε_0 is the vacuum dielectric constant, 8.854×10^{-12} F m^{-1}; d is the diameter of the coupled electrodes, 0.01 m.

References:

1. Tian E, Gao Y, Mo J. Electrostatically assisted air coarse filtration for energy efficient ambient particles removal: long-term performance in real environment and influencing factors. *Build Environ* **164**, 106348 (2019).